Recent ARPES experiments on quasi-1D bulk materials and artificial structures

2009 J. Phys.: Condens. Matter 21 023201

(http://iopscience.iop.org/0953-8984/21/2/023201)

IOP PUBLISHING JOURNAL OF PHYSICS: CONDENSED MATTER

J. Phys.: Condens. Matter **21** (2009) 023201 (24pp) doi:10.1088/0953-8984/21/2/023201

TOPICAL REVIEW

Recent ARPES experiments on quasi-1D bulk materials and artificial structures

M Grioni[1], S Pons[1,2] and E Frantzeskakis[1]

[1] Institut de Physique des Nanostructures, École Polytechnique Fédérale de Lausanne—EPFL, CH-1015 Lausanne, Switzerland

[2] Laboratoire de Physique des Matériaux, Nancy-Université, CNRS, Boulevard des Aiguillettes, BP 239, F-54506 Vandoeuvre lès Nancy, France

E-mail: marco.grioni@epfl.ch

Received 22 July 2008, in final form 16 September 2008
Published 9 December 2008
Online at stacks.iop.org/JPhysCM/21/023201

Abstract

The spectroscopy of quasi-one-dimensional (1D) systems has been a subject of strong interest since the first experimental observations of unusual line shapes in the early 1990s. Angle-resolved photoemission (ARPES) measurements performed with increasing accuracy have greatly broadened our knowledge of the properties of bulk 1D materials and, more recently, of artificial 1D structures. They have yielded a direct view of 1D bands, of open Fermi surfaces, and of characteristic instabilities. They have also provided unique microscopic evidence for the non-conventional, non-Fermi-liquid, behavior predicted by theory, and for strong and singular interactions. Here we briefly review some of the remarkable experimental results obtained in the last decade.

(Some figures in this article are in colour only in the electronic version)

Contents

1. Introduction

Elementary textbooks on solid-state physics often discuss the simple case of a *one-dimensional* (1D) *metal* as a convenient way to introduce basic notions on the electronic structure of solids, without the unnecessary geometrical complexities of three-dimensional (3D) systems. It is generally pointed out that such a simple, idealized, model has no practical realization and, for this reason, cannot reproduce many details of 'real' materials. But this is only partially true. Chemists and material scientists have been able to synthesize a large number of inorganic and organic compounds, which exhibit very anisotropic physical properties, and effectively behave—in some limited temperature and energy range—as 1D conductors. In an extreme 'bottom-up' approach, truly 1D systems, with tunable lattice spacings and interaction strengths, can even be created by confining ultracold atoms in appropriate optical lattices (Moritz *et al* 2005).

The 1D 'toy model' has a deeper conceptual limitation. While it mimics the properties of real 3D metals, it cannot possibly describe 1D (or quasi-1D) systems. The reasons

are twofold. Firstly, real quasi-1D systems invariably exhibit instabilities which eventually lead to broken-symmetry phases. The ground state is therefore not a metal, and may exhibit a charge-(CDW) or spin-density wave (SDW), or superconductivity (SC), or again be a Mott insulator (Grüner 1994). Secondly, electron–electron and electron–phonon interactions strongly affect the properties of 1D systems even in their 'normal' state. The consequences of the peculiar electronic correlations are particularly dramatic. Quasi-particle (QP) excitations are washed out and replaced by collective (charge and spin) modes. The usual Landau Fermi liquid (FL) paradigm for interacting fermions is replaced by the so-called Luttinger liquid (LL), or by related models with gaps in the charge or spin channels (Giamarchi 2003).

Photoelectron spectroscopy (PES), namely with angular (i.e. momentum) resolution (ARPES), has proven to be a powerful probe of these intriguing 1D properties. ARPES can measure the overall band structure of a solid, but can also address specific electronic states at selected energies and momenta. In particular, it can measure in great detail the shape and size of the Fermi surface (FS), and its partial or complete disruption following an electronic instability. The close tie with theory makes it generally useful in all systems which cannot be effectively described in terms of non-interacting particles. The electron removal spectrum measured by ARPES gives in fact direct access to the one-particle spectral function $A(k, \omega)$. This fundamental theoretical quantity contains exhaustive information on the single-particle excitations of a many-body system, and therefore on the nature and the strength of the interactions (Mahan 1986). In a Fermi liquid, it yields the energy, lifetime, and correlation length of the QPs, which determine the thermodynamic properties of the material (Nozières 1964). In 1D systems, where the Fermi liquid breaks down, $A(k, \omega)$ is expected to reflect in various ways the absence of coherent QP excitations, and to bear characteristic signatures of collective spin and charge excitations (Meden and Schonhammer 1992, Voit 1993).

When high-resolution PES and ARPES data on 1D metallic systems first showed a strong suppression of spectral weight near the Fermi level (E_F) (Dardel *et al* 1991), this unusual observation came as a surprise to many experimentalists used to 'normal' metals. With hindsight, although indeed unusual, this result should not have been unexpected. As briefly mentioned already, various mechanisms can lead to a suppression of the normal metallic signatures in 1D systems. They include the predicted breakdown of the Fermi liquid, but also transitions to insulating ground states, and precursor 'pseudogapped' phases well above the corresponding phase transition temperatures. Over the years ARPES experiments have explored these different facets of the problem. On the one hand the band dispersion, the properties of the Fermi surface, and their changes in the broken-symmetry states have been determined in many real quasi-1D materials. On the other hand, ARPES has been utilized to search for the spectral fingerprints of non-Fermi-liquid behavior. The two complementary aspects are illustrated in this article. One further line of research has emerged in recent years. It concerns the properties of quantum wires fabricated at surfaces. These artificial structures have rapidly become important model systems where parameters can be more easily tuned to explore broader regions of the phase diagram of correlated 1D electrons. Again, ARPES has produced a wealth of interesting results.

The scope of this brief review is mainly limited to experimental spectroscopic results from the past 10 years. Many important theoretical aspects of correlated materials, as well as the general concepts of instabilities in 1D, have been omitted on purpose. They are discussed in great detail in excellent books (Giamarchi 2003, Grüner 1994) and review papers (Voit 1993, Allen 2002). It would also be impossible to provide appropriate background information for all case studies discussed here, and the reader is referred to the references in the original papers. Finally, we will not consider here 2D systems—surfaces and interfaces—which exhibit 1D-like anomalies in the phonon and electron spectrum due to peculiar nesting properties of their Fermi surfaces. A recent review on this interesting topic is found in (Kröger 2006).

The structure of the paper is the following. Bulk 1D materials are discussed in section 2, where the important cases of transition metal (TM) chalcogenide compounds, of metallic and insulating oxides, and of organic systems are illustrated. Section 3 gives a brief introduction to 1D systems at metal surfaces. Atomic wires on silicon are discussed in section 4.

2. Bulk quasi-1D compounds

2.1. Transition metal chalcogenides

The chain-like structure of transition metal trichalcogenides MX_3 (X = S, Se, Te) often leads to strongly anisotropic electronic properties, and to characteristic 1D instabilities, which are usually associated with the nesting properties of their Fermi surface (FS) (Grüner 1994). These materials are all structurally related, with one, two or three inequivalent chains built from MX_6 prisms running along the crystallographic *b*-axis.

The importance and the subtleties of the nesting properties in the presence of a complex, multi-sheet Fermi surface are well illustrated by the case of $NbSe_3$. This material exhibits transitions at $T_1 = 145$ K and $T_2 = 59$ K to incommensurate CDWs with distinct wavevectors $\mathbf{q}_1$ and $\mathbf{q}_2$. Each transition removes parts of the FS, and leads to giant resistivity anomalies, but the material remains metallic at all temperatures, showing that the removal is not complete. The dimensionality of the electronic structure at the Fermi level (E_F) is determined by the dominant Nb–Nb interactions along the chains. As a consequence, the structural and electronic anisotropies coincide, and 1D-like open FS sheets are formed perpendicular to the chain axis. First-principles density functional theory (DFT) calculations predict five bands crossing E_F, and therefore five FS sheets. Four of them are well nested either along the chain axis, with wavevector $\mathbf{q}_1$, or diagonally, with wavevector $\mathbf{q}_2$.

ARPES data collected at RT, in the normal state, show a shallow feature with parabolic dispersion corresponding to unresolved Nb 4d bands in the DFT calculation (Schäfer

et al 2001). The extrapolated Fermi level crossing (at $k_F = \pm 0.22$ Å^{-1}) identifies a nesting vector $q = 2k_F$ in excellent agreement with $\mathbf{q}_1$, but the band bends away from E_F before the actual crossing. The avoided crossing indicates that a pseudogap is already open at RT, which is below the estimated mean-field transition temperature T_{MF} for $NbSe_3$, but well above T_1. As in other 1D CDW materials, it reflects the formation of CDW segments fluctuating in space and time. The corresponding correlation length $\xi = (\hbar v_F/\pi k_B T)$ is estimated at 30 Å at RT. A symmetric 'shadow band' is observed beyond k_F, reflecting the underlying CDW periodicity already present in the fluctuating CDW segments. The intensity of the shadow band is however much smaller than that of the main band. This can be understood considering that the spectral weight distribution is determined by the strength of the superlattice potential associated with the CDW, which is also much smaller than the lattice potential (Voit *et al* 2000).

Data measured at $T = 15$ K $< T_2$ display an additional CDW periodicity, and illustrate the removal of those parts of the FS that are diagonally nested by $\mathbf{q}_2$. However, non-nested portions of the FS are predicted by the DFT band structure, and this is indeed confirmed by the experiment. The details of the ARPES line shapes are surprising, both at the removed and at the remaining FS locations. At the former, the spectral intensity is strongly suppressed near E_F, but pseudogaps, rather than clear gaps, are observed. The ratio of the two pseudogaps $\Delta_1/\Delta_2 = (110/45)$ is in good agreement with the ratio of the CDW transition temperatures (T_1/T_2). At the locations of the FS that are neither nested by $\mathbf{q}_1$ nor by $\mathbf{q}_2$, QP features are observed to disperse all the way to E_F, but with diminished coherent intensity, and a non-dispersing satellite appears at a binding energy $\varepsilon_0 \approx 90$ meV (figure 1) (Schäfer *et al* 2003). There is a clear analogy with the spectral signatures of QPs coupled to a phonon mode (Hengsberger *et al* 1999), or more generally to a bosonic excitation of energy ε_0. A simple phonon interpretation cannot be reconciled with the fact that ε_0 is roughly three times larger than the largest phonons energy in $NbSe_3$. On the other hand, ε_0 is just equal to the full gap $2\Delta_2$ associated with the $T = T_2$ transition, which suggests that the spectral renormalization is a consequence of the CDW. This is further supported by the fact that the satellite cannot be detected at $T = 100$ K $> T_2$. These considerations, which illustrate the complexities underlying the formation of broken-symmetry states in 1D materials, are largely phenomenological. Further theoretical analysis is necessary to clarify the nature of the coupled mode, and to develop a coherent scenario of the instabilities. The data nevertheless show that detailed ARPES measurements with high momentum and energy resolution can unveil subtle and important aspects of the electronic structure of 1D materials.

The closely related semimetallic compound $TaSe_3$ does not exhibit comparable anomalies in the transport properties, but the unusual temperature dependence of the resistivity suggests that it is close to a CDW instability. A rather unique feature of the electronic structure of this material, as measured by ARPES, is a parabolic band with a small negative effective mass, which defines a small hole pocket at the center of the Brillouin zone (BZ). The top of the band however appears to

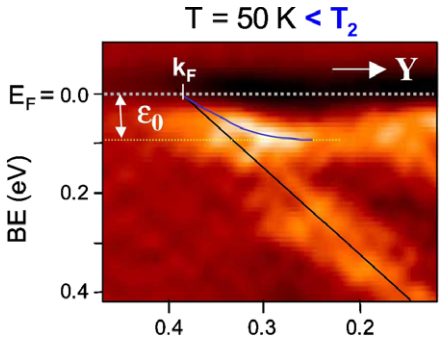

Figure 1. ARPES intensity map of the renormalized band dispersion of $NbSe_3$ near the Fermi surface, just below the $T_2 = 59$ K CDW transition. Reprinted with permission from Schäfer *et al* (2003). Copyright 2003 by the American Physical Society.

be truncated, yielding a narrow flat region of large spectral weight 60 meV below E_F. Only a tail of the main spectral peak extends to the Fermi level, ensuring the metallic conductivity of $TaSe_3$ (Perucchi *et al* 2004). The nesting properties of the corresponding FS remain to be investigated.

$ZrTe_3$ is an interesting and anomalous case in the MX_3 family. It exhibits a CDW instability at $T_P = 63$ K, but remains metallic down to 2 K, where it enters a superconducting phase. With one d electron less to accommodate than in the Nb or Ta trichalcogenides, the Fermi level moves down in the band structure, and into the Te 5p manifold. Transverse interchain interactions involving neighboring Te ions then lead to the formation of bands with 1D character which disperse not along the chains, but in the perpendicular direction. Band structure calculations predict a complex multi-sheet Fermi surface with coexisting 1D and 3D characters. Namely, a hole-like 3D Fermi sheet is centered at Γ, while closely spaced quasi-1D open electron-like sheets run along the BZ boundary. These warped 1D FS sheets are partially nested by a wavevector which is compatible with the CDW wavevector. The overall features of the predicted band structure, namely the existence of a very shallow electron pocket at $(\pi/a, 0)$, associated with the flat FS sheets, were detected by an initial ARPES survey (Søndergaard *et al* 2003), and later confirmed by an extensive k-space mapping (Starowicz *et al* 2007).

It was subsequently shown that the electron pocket is associated with a van Hove singularity (vHs) as predicted by theory (Yokoya *et al* 2005). The vHs however is too far from the FS to be directly involved in the CDW formation. Changes of the electronic structure induced by the CDW are revealed by ARPES measurements performed over a broad temperature range. The ARPES line shape at the 3D FS remains unchanged, except for a trivial sharpening at low temperature. Clear temperature changes are instead observed at the 1D FS sheets. At the corner $(\pi/a, \pi/b)$ of the BZ a continuous shift of spectral weight away from the Fermi energy is observed with decreasing temperature. The loss of intensity at E_F is accompanied by the growth of a broad peak centered at 150 meV. The spectra, divided by the Fermi function (figure 2(a), top), reflect the progressive opening of a pseudogap within 70 meV of E_F below ≈ 200 K. The ARPES data therefore illustrate the expected influence of

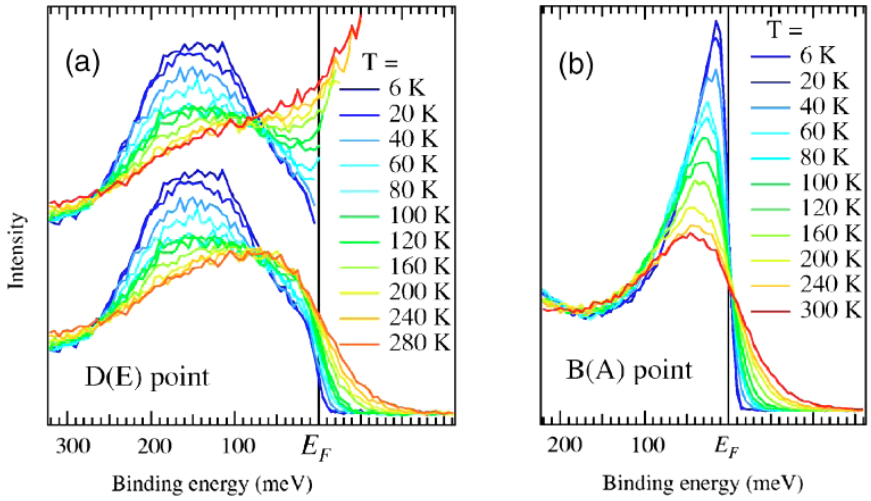

Figure 2. Temperature dependence of the ARPES spectra of $ZrTe_3$ at selected points of the Fermi surface. After normalization by the T-dependent Fermi–Dirac function, the data show the opening of a gap at the 1D FS sheet (a), while only a trivial spectral sharpening is seen at the 3D sheet (b). Reprinted with permission from Yokoya *et al* (2005). Copyright 2005 by the American Physical Society.

CDW fluctuations in the 'normal' state below the mean-field transition temperature $T_{MF} \approx 3T_P$ (Lee *et al* 1973). However, the binding energy of the new peak structure is not only much larger than the Peierls energy scale $\Delta \approx 3.5\, k_B T_P \approx 20$ meV, but also two to three times larger than the energy scale associated with T_{MF}. Moreover, the gap opening is incomplete, as some residual intensity is present at E_F even at 6 K, well into the CDW state. Both observations are unusual for 1D CDW systems. The situation is quite different at the $(\pi/a, 0)$ point of the FS, where the QP peak sharpens and grows in intensity with decreasing temperature (figure 2(b)). There is no sign of a gap developing at low temperature, consistent with the fact that nesting is spoiled in this part of the FS by warping, i.e. by a deviation from strict one-dimensionality. The sharp peak at E_F contrasts with the usual observation of suppressed spectral weight in quasi-1D metals. It indicates increasing QP coherence at lower temperature, as in normal (3D) metals. Although the CDW transition has a 3D character even in a quasi-1D system, the behavior of $ZrTe_3$ is unusual, because the resulting CDW state is metallic. The increasing coherence could be a consequence of the developing pseudogap, which reduces phase space for QP scattering.

$(TaSe_4)_2I$ is a prototypical 1D compound, with a CDW transition at $T_P = 263$ K. In an ionic picture, 0.5 electrons would be transferred from each Ta (d^1) atom to the anions. The Ta 5d conduction band would be exactly quarter filled, setting up the conditions for a commensurate CDW with period λ_{CDW} equal to four times the Ta–Ta distance d along the chain. In reality, charge transfer to the iodine ions is not complete and band filling is slightly larger, so that the CDW is incommensurate, with $\lambda_{CDW} \approx 3.7d$. The FS is open and consists of parallel and slightly warped planes perpendicular to the chain axis (Hüfner *et al* 1999). Interestingly, high-resolution ARPES data exhibit signatures of both the lattice and the CDW periodicities, and well developed shadow bands (Voit *et al* 2000). The temperature dependence of the spectra clearly reflects the growth of the CDW below T_P. Namely, the

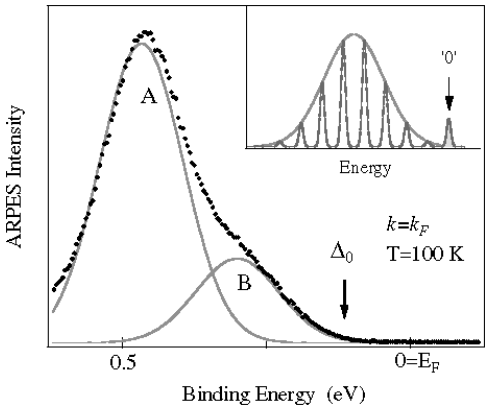

Figure 3. ARPES spectrum of $(TaSe_4)_2I$ at $k = k_F$, in the CDW phase. The broad line shape is decomposed into two features corresponding to the B and AB bands. Inset: schematic 'polaronic' line shape, showing the strong renormalization of the coherent ('0') QP peak. Reprinted with permission from Perfetti *et al* (2001). Copyright 2001 by the American Physical Society.

spectral leading edge progressively shifts away from E_F, and the total shift $\Delta E = 0.12$ eV between T_P and the saturation value at $T \approx 100$ K coincides with estimates of the CDW gap from optics and transport (Perfetti *et al* 2001). Nevertheless, the broad spectral line shape is inconsistent with a standard Peierls scenario (figure 3). In particular, fluctuations above the actual transition temperature cannot justify the loss of intensity well beyond the gap energy scale.

The non-trivial temperature evolution of the ARPES line shape suggests that the spectral leading edge, rather than the peak position, may be related to the QP energy. This requires a scenario where the QP signal is dramatically reduced, and spectral weight is redistributed over a broad energy range. Electronic correlations can transfer spectral weight from the coherent QP peak to the incoherent part of the spectral function, over a broad energy range, determined

by the specific nature of the interaction. The reduction of the QP spectral weight can be as large as 1000 in extreme cases like the heavy fermion compounds, but such strong electronic interactions do not seem compatible with the properties of $(TaSe_4)_2I$. The electron–phonon interaction, which is large in Peierls materials, can also drastically modify the spectral line shape. Some insight is provided by the simple model of one electron coupled to a single harmonic oscillator of frequency Ω (figure 3, inset), similar to the Franck–Condon problem in molecules. The electron removal spectrum has a high energy 'zero phonon' (0) peak, followed by a progression of equally spaced satellites with a Poissonian envelope, corresponding to the excited vibrational final states of the oscillator. The (0) peak represents the coherent QP peak of the model, while the satellites are the 'incoherent' part of the spectrum, and the relative weight of the coherent and incoherent parts depends on the strength of the interaction. In the strong coupling, adiabatic ($\hbar\Omega \ll t$, the electron hopping integral) limit the satellites merge into a single Gaussian peak at an energy $E \approx \langle n \rangle \hbar\Omega$ below the (0) peak, where $\langle n \rangle$ is the average number of vibrations 'dressing' the electron. The heavy renormalized carriers are small polarons, i.e. electrons moving coherently with the distortion they induce in the lattice. The coherent weight is exponentially suppressed with $\langle n \rangle$, and may even not be detectable at the leading edge of the spectrum. This spectral function is a qualitative guideline to describe electrons strongly interacting with the lattice in a real solid. A similar picture had originally been proposed for the 2D giant magnetoresistance manganites (Dessau *et al* 1998), and more recently utilized for the underdoped superconducting cuprates (Shen *et al* 2004).

Figure 3 illustrates a fit to the ARPES spectrum of $(TaSe_4)_2I$ with two polaronic line shapes accounting for the bonding (B) and antibonding (AB) bands predicted by band theory in this compound. It is clear that in the polaronic scenario the 'A' and 'B' features of the experimental spectrum are only indirectly related to the energies of the corresponding QPs, which are hidden under the tails of the two Gaussian line shapes. For reasonable values of the relevant phonon energies (10–35 meV), the fit yields $\langle n \rangle \approx 5$–$15$, close to $\langle n \rangle \approx 10$ obtained from independent optical measurements. Interestingly, such a strong intensity renormalization is not incompatible with a broad ARPES dispersion, as shown by recent theory (Perebeinos and Allen 2000, Mishchenko and Nagaosa 2004). This can be understood with a simple qualitative argument. Immediately after being created the photohole sees a 'frozen' lattice, where it can disperse with the velocity—and bandwidth—calculated by band theory. Quite rapidly, however, the hole is dressed by phonons and the small polaron—with its small coherent spectral weight—is formed. Realistic model calculations show that the corresponding, mostly incoherent, spectral weight is then peaked around the predicted band dispersion, in agreement with the simple picture of figure 3.

Spectral signatures of a superlattice periodicity were observed in the closely related insulating compound $(NbSe_4)_3I$, which exhibits a temperature-independent commensurate distortion. The wavelength of the distortion along the Nb chains is three times the Nb–Nb distance d, i.e. exactly the value which would be expected in a Peierls scenario for the one-third-filled valence band. The actual periodicity is actually $6d$, due to the spiral arrangement of the planar (Se_4) units surrounding each chain. The dispersion measured by ARPES has the periodicity of the distorted chain, with maxima at $k = \pi/3d$, but also weaker shadow bands corresponding to backfolding at $k = \pi/6d$. This shows that scattering of electrons from the potential of the Se_4 units is not negligible (Vescoli *et al* 2000). The spectral line shape is quite similar to the polaronic line shape of $(TaSe_4)_2I$, and suggests a similar interpretation.

The 1D ternary semiconducting chalcogenides $TlGaSe_2$ and $TlInTe_2$, which are also of interest in view of the large values of their Seebeck coefficients, have also been recently studied by ARPES (Okazaki *et al* 2001, Mimura *et al* 2007). The data show sizeable dispersions in the perpendicular direction in spite of the structural 1D character of these compounds. They are explained by interchain interactions associated with the large number (eight) of Se(Te) atoms surrounding each Tl ion. Strong temperature dependences of the ARPES spectra have been observed, namely a reduction of the energy separation between the Fermi level and the top of the valence band with lowering temperature. This suggests a temperature-dependent pinning level in the semiconducting gap, and it is interpreted as an indirect consequence of an incommensurate modulation appearing below RT. The same incommensurate modulation also opens mini-gaps in the band structure, in agreement with theoretical predictions (Voit *et al* 2000). Notice however that the insulator–insulator transition observed in these materials cannot be directly assimilated to the Fermi surface driven 1D Peierls instability.

2.2. Oxides

Among a broad range of physical properties, transition metal oxides may also exhibit 1D electronic behavior and characteristic instabilities. A typical example is the molybdenum 'blue bronze' $K_{0.3}MoO_3$, a prototypical CDW compound. Its spectral properties have been intensively studied since the first observations of unusual line shapes by high-resolution PES (Dardel *et al* 1991). The structural building blocks of this material are parallel chains of MoO_6 octahedra running along the crystallographic b-axis. The FS consists of two warped open sheets with opposite curvature. They are derived from bonding (B) and antibonding (AB) combinations of Mo 4d states on neighboring chains. The B and AB sheets are alternatively nested with the same wavevector, yielding a single incommensurate CDW below $T_P = 180$ K. The CDW eventually locks into a commensurate state below ≈ 100 K with a modulation vector $\mathbf{q}_{CDW} = (\mathbf{a}^*, 0.75\ \mathbf{b}^*, 0.5\ \mathbf{c}^*)$. ARPES data in the normal state above T_P show the dispersing B and AB bands, but also a dramatic reduction of their spectral weight as they approach E_F. An underlying open FS, with distinct Fermi wavevectors k_F(A) and k_F(AB), is nonetheless revealed by integrating the ARPES signal over a narrow energy window below E_F (Gweon *et al* 1996). The separation between the two FS sheets decreases by $\approx$10% between 300 and 40 K. The nesting vector $q = k_F(B) + k_F(AB)$ reproduces the temperature dependence of q_{CDW},

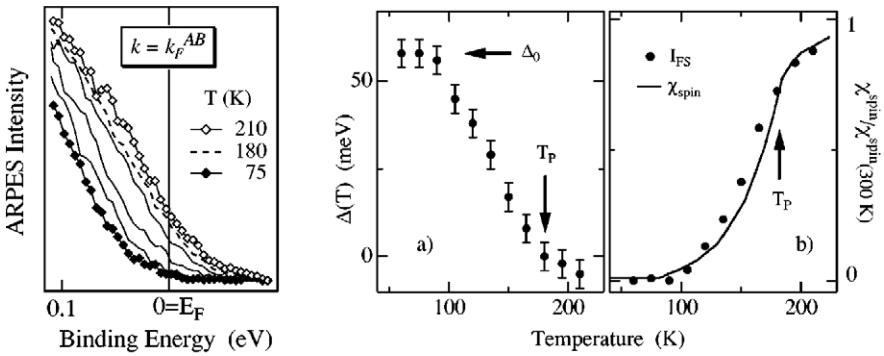

Figure 4. Left: temperature dependence of the ARPES spectrum of the 'blue bronze' $K_{0.3}MoO_3$, measured at $k = k_F(AB)$, from which the CDW (pseudo)gap $\Delta(T)$ shown in the center panel is derived. Right: the T-dependence of the ARPES intensity at the Fermi surface is compared with the spin susceptibility. Reprinted with permission from Perfetti *et al* (2002). Copyright 2002 by the American Physical Society.

thus demonstrating the electronic nature of the temperature dependence seen in neutron and x-ray scattering experiments (Fedorov *et al* 2000). A full mapping of the FS shows that the open sheets are warped, especially that corresponding to the B band. As temperature is lowered, the warping is reduced and the nesting is enhanced (Ando *et al* 2005). The opening of the Peierls gap has been followed by recording the position of the spectral leading edge at the Fermi wavevectors. The temperature dependence for $k = k_F(AB)$ is shown in figure 4 (left); the spectra at $k = k_F(A)$ exhibit a similar evolution. Both bands progressively shift away from E_F, to a saturation value $\Delta_0 = 60$ meV (figure 4 (center)), which is consistent with half of the Peierls gap, similar to the case of $(TaSe_4)_2I$ (Perfetti *et al* 2002). This phenomenological analysis is also supported by the observation that the ARPES intensity at the Fermi surface follows quite closely the T-dependence of the spin susceptibility (figure 4 (right)). This quantity is proportional to the QP weight. It reflects the opening of a fluctuation-induced pseudogap above, and of a real Peierls gap below, T_P.

The strong spectral weight renormalization near E_F, and large discrepancies between the measured bandwidths and the results of early model calculations, have been interpreted as possible signatures of the Luttinger liquid behavior predicted for strictly 1D fermionic systems. A difficulty with this interpretation is the lack of clear evidence for strong electron–electron interactions in the blue bronze. Moreover, the discrepancy with the ARPES dispersion has been removed by more recent density functional calculations (DFT) (Mozos *et al* 2002). A polaronic scenario, similar to the case of $(TaSe_4)_2I$ discussed above, may be more appropriate for this CDW material (Perfetti *et al* 2002). A very similar 'polaronic' spectral line shape has been observed in the related insulating 'red bronze' $K_{0.33}MoO_6$ (Mitrovic *et al* 2004). Here, due to a different arrangement of the MoO_6 octahedra, the valence band consists of a single branch. It is observed by ARPES to disperse with the periodicity of a static distortion along the chains. This suggests a common 'Peierls' scenario for the two compounds, with a very high transition temperature for the red bronze, which would then remain in the broken-symmetry state in the whole temperature range of stability.

The Mo 'purple bronzes' AMo_6O_{17} (A = Na, K) are quasi-2D materials. Their FSs are closed, even if they can ideally be decomposed into three 1D-like pairs of parallel sheets which lead to CDW instabilities (hidden nesting) (Whangbo *et al* 1991, Gweon *et al* 1996). The Li purple bronze—whose actual stoichiometry is $Li_{0.9}Mo_6O_{17}$—exceptionally exhibits 1D metallic behavior over a broad temperature range. At $T = 24$ K the resistivity has a rapid upturn, but no structural signs of a CDW instability have been reported. The corresponding energy gap, if any, must be smaller than 1 meV. Finally, superconductivity sets in at 1.9 K. The spectroscopic properties of the Li purple bronze have been the subject of much interest and debate for more than one decade. Thanks to the absence of instabilities down to very low temperatures, and to the very small size of any possible pseudogap in the metallic phase, this compound provides an excellent opportunity to test the non-Fermi-liquid spectral properties of 1D conductors. The strongly 1D character of the underlying FS, with the two essentially flat parallel sheets predicted by band theory for this material, has been confirmed by ARPES data (Denlinger *et al* 1999). The overall band structure also agrees with that of an extended Hückel calculation, except for a discrepancy on the bandwidth, similar to that initially reported for the blue bronze. The data show a very low spectral intensity at E_F, and a line shape which is incompatible with that of a normal metal.

Measurements performed with a better momentum resolution by a second group have yielded contrasting data and a very different interpretation (Xue *et al* 1999). They show sizeable intensity at the Fermi surface and, after a momentum integration of the spectra over ≈15% of the BZ, an apparent metallic Fermi step at RT. The same data show at k_F a large (40 meV) shift of the leading edge of the spectrum between 300 and 17 K, which was interpreted as the signature of the opening of an unexpected 80 meV gap. However, the reports of a metallic spectrum and of a gap opening have not been confirmed by subsequent high-resolution measurements performed by the first group (Gweon *et al* 2001). The more recent data are compatible with earlier, less detailed results from single crystals of the same origin (Grioni *et al* 1996). Sample issues may therefore play a role in this discrepancy, which remains unresolved.

The perovskite-related oxides $SrNbO_{(3.5-x)}$ exhibit a layered structure built from slabs of NbO_6 octahedra, which are continuously connected via their apical oxygens and form infinite chains along the crystallographic a-axis. For $x \approx 0.1$ the states determining the Fermi surface are essentially localized on the Nb–O–Nb chain at the center of the slab, so that these compounds exhibit genuine 1D properties. Various compositions around $x = 0.1$ have been studied by ARPES and optical spectroscopy (Kuntscher *et al* 2000, 2002). The ARPES dispersion identifies open Fermi surfaces with a strong 1D character, and a nesting vector $q = \pi/3$. Shadow bands and shadow FSs are also observed, corresponding to a (2×1) structural reconstruction already identified in diffraction experiments. High-resolution measurements for $x = 0.09$ actually show that a very small ($\approx$4 meV) gap is open at 25 K. This is the spectroscopic counterpart of a low-temperature upturn of the resistivity along the chain axis. It is unlikely that the gap is due to electronic correlations, which are not expected to be strong in 4d transition metal (TM) systems, particularly for a commensurability different from 1/2. A Peierls instability towards a still undetected CDW phase cannot be ruled out, but the small value of the gap is unusual. The weak-coupling BCS relation $2\Delta(0) \approx 3.5\, k_B T_c$, which is also valid for CDWs, yields a mean-field transition at $T_{MF} \approx 40$ K. The actual (3D) phase transition would occur as usual in 1D systems at a lower $T_P \approx T_{MF}/3$. This is inconsistent with the strong deviation from metallic behavior already observed below $\approx$55 K. Therefore a simple Peierls scenario cannot quantitatively reconcile the temperature and spectroscopic energy scales.

V_6O_{13} is an inhomogeneous mixed-valent compound with a metal–insulator (MI) transition at $T_{MI} = 150$ K, and a further magnetic (paramagnetic–antiferromagnetic) transition at 50 K. It has a layered (2D) structure based on parallel sheets of VO_6 octahedra. Within the sheets, two kinds of 1D zigzag chains of octahedra running along the b-axis are at the origin of strongly anisotropic transport properties. In the metallic phase (M), all V atoms of chain (1) have a formal valence V^{4+} (d^1), while V^{4+} and V^{5+} (d^0) sites alternate along chain (2). Conventional ARPES measurements (Eguchi *et al* 2002) show, in the M phase, a 1D band dispersing only along the chain direction, with a bandwidth of $\approx$0.2 eV. This band, attributed to the mixed V^{4+}–V^{5+} chain (2), forms a small electron pocket around Γ, but the ARPES intensity is strongly suppressed near E_F. The spectra also show a stronger incoherent feature at 0.8 eV, derived from chain (1), which is assigned to a lower Hubbard band as in other V oxides. At T_{MI} the shallow band disappears, leaving a 0.2 eV gapped region below E_F. Both in the M and in the insulating (I) phases the spectra exhibit the broad features that are typical for TM oxides. A coexistence of dispersive coherent and incoherent features in the M phase is seen also in soft x-ray ($h\nu = 515$ eV) ARPES measurements (Suga *et al* 2004). These less surface-sensitive data confirm the collapse of the QP band below T_{MI}, even if the spectral details are somewhat different. In particular, they reveal a new incoherent feature at 1.5 eV in the I phase, which is interpreted in terms of a charge redistribution within the V sites.

β-$Na_{0.33}V_2O_5$ is another inhomogeneous mixed-valent compound which behaves as a quasi-1D metal at high temperature. It exhibits an MI transition at T_{MI} =135K accompanied by charge ordering on the inequivalent V ions and, remarkably, superconductivity under pressure below 8 K. Its 1D electronic character is associated with three distinct 1D structural units, namely infinite zigzag chains, two-leg ladders of VO_6 octahedra, and chains of VO_5 pyramids. ARPES data (Okazaki *et al* 2004) show a broad Gaussian-like feature with V 3d character centered at $\approx$0.9 eV. Its leading edge has a vanishingly small intensity at E_F, and disperses only along the chain direction, with a minimum binding energy at $k = \pi/4$. This periodicity indicates that charge carriers donated by the Na ions either equally dope one chain and the ladders, or only the ladders, in the limit of very small hybridization between the rungs. The broad line shape is attributed to a strong electron–phonon interaction. This scenario is then quite different from that invoked for the pristine 1D insulating compound NaV_2O_5 (Kobayashi *et al* 1998). In that case, similarly broad Gaussian-like features were observed to disperse and reach a minimum binding energy at $k = \pi/2$, and the spectra were interpreted within a half-filled Hubbard model, appropriate for strongly correlated 1D electrons.

Edge-sharing infinite chains of $Ti(O_4Cl_2)$ octahedra in the insulating compound TiOCl represent a good practical realization of $S = 1/2$ Heisenberg chains, with a large direct exchange energy $J = 660$ meV. This quantum magnet has been studied for a sudden drop of the susceptibility at $T_{SP} = 67$ K, interpreted as an unusual first-order spin–Peierls transition, leading to a doubled periodicity along the chains. PES data collected at $T > T_{SP}$ and LDA + U calculations (Hoinkis *et al* 2005) identify a dispersive valence band of pure d_{xy} character. Symmetry-selective polarized ARPES spectra did not find evidence for mixing of this band with the $d_{xz,yz}$ bands of the Ti 3d manifold, which the calculation places at $\approx$100 meV higher energy. This observation rules out Jahn–Teller orbital fluctuations as a possible origin of the transition. The ARPES spectra show a rather broad feature, whose peak disperses along the chain axis, reaching a minimum binding energy at $k = \pi/2$, and then receding from E_F for larger momenta. The LDA + U calculations for the dimerized structure do not reproduce the asymmetric spectral weight distribution around $\pi/2$. A single-band 1D Hubbard model at half filling comes closer to reproducing the experimental results. However, the data do not exhibit the signatures of spin–charge separation predicted by theory in 1D (Voit 1994).

$LiCu_2O_2$ is another insulating $S = 1/2$ chain compound, with Cu^{2+} (d^9) local spins. The elementary structural units are edge-sharing CuO_4 plaquettes, which form infinite chains running along the crystallographic b-axis. This compound was recently studied by a combination of angle-integrated and angle-resolved photoemission (Papagno *et al* 2006). The highest-lying feature in PES is attributed to the 'Zhang–Rice singlet' (ZRS) band built from local $d^9\underline{L}$ states ($\underline{L}$ is a ligand hole). The dispersion of the ZRS, namely its maximum at $k = \pi/2$, is not reproduced by the LDA band structure calculations. Moreover, a closer inspection reveals that two distinct features underline the broad line shape. Again, the data are qualitatively consistent with descriptions based on an effective half-filled 1D Hubbard or t–J model, which confirms the importance of

electronic correlations in the low-dimensional cuprates. From the bandwidths of the two ARPES components, the hopping parameter $t \approx 0.37$ eV and exchange parameter $J \approx 35$ meV can be directly estimated, albeit with a large uncertainty on the latter, due to the difficulty of extracting with high accuracy the dispersion of the shallower component.

2.3. Beyond the Fermi liquid: spin–charge separation

The most distinctive spectral signature of the breakdown of the Fermi liquid in a 1D system is the absence of coherent QP peaks in the spectral function. They are replaced in a Luttinger liquid (LL) scenario by distinct singularities dispersing with different velocities (Voit 1994). The incoherent 'spinon' and 'holon' spectral features represent the collective spin and charge excitations of the correlated 1D system, and reflect spin–charge separation. These LL features have proven to be fairly elusive in metallic compounds, and it is actually unsure that the appropriate conditions for their straightforward observation can be realized in real metallic systems. So far, the clearest observation of spin–charge separation by ARPES has come not from metals, but from insulating 1D compounds, where a half-filled band is gapped by electronic correlations. Because of the energy gap these systems, even in the strict 1D limit, are not Luttinger liquids, but rather 'Luther–Emery' liquids, which belong to a different universality class. Nonetheless, their low-energy excitations exhibit similar momentum dependence and line shapes (Voit 1998). The spectra are expected to exhibit some distinctive features: (i) a 'holon' singularity with a symmetric dispersion around its maximum at $k = \pi/2$; (ii) a shallower 'spinon' singularity for $0 < k < \pi/2$; the spinon and holon bandwidths are $\pi J/2$ and respectively $2t$ in a t–J model; (iii) a continuum between the holon and spinon edges, which reflects the possibility of decomposing in many different ways a photohole into a holon and a spinon.

Features (i) and (iii) were first identified in the ARPES spectra of the insulating cuprate $SrCuO_2$ (Kim *et al* 1996, 1997). The 1D properties of this material are associated with infinite double chains of Cu^{2+} ions built from edge-sharing CuO_4 plaquettes. Similar results were obtained shortly afterward in Sr_2CuO_3, another 1D AFM cuprate insulator with a simpler single-chain structure derived from corner-sharing CuO_4 plaquettes (Fujisawa *et al* 1998). In both materials the broad spectral line shape was compatible with underlying and separately dispersing features in the first half of the BZ, although a direct identification of the spinon and holon was not possible. A remarkable result was the observation that the total dispersion of the high-binding-energy holon edge of the spectrum ($\approx$1 eV) was about three times larger than the bandwidth of $Sr_2CuCl_2O_2$, a reference 2D AFM cuprate with very similar CuO_4 elementary structural units. This is in sharp contrast with standard band theory, which would predict a larger—by a factor of two—bandwidth in 2D due to the correspondingly larger number of neighbors. The results, obtained on two different systems, could not claim a complete agreement with the predicted 1D spectral properties, but did reveal the incompatibility with a standard '2D' or '3D' description, and showed that the 1D Luttinger scenario was at least a plausible one.

A real breakthrough has recently been achieved with an improved set of data on $SrCuO_2$, where for the first time clearly separate features can be distinguished in the ARPES spectral line (figure 5, left) (Kim *et al* 2006). The use of a relatively high photon energy (85 eV) in the new experiment has two important advantages. Firstly, it enhances the relative cross section of the hybrid Cu–O band with respect to the partially overlapping main O 2p feature at higher-binding energy, which dominates the prior low-energy data. Secondly, it allows a broader momentum range to be explored. Both aspects contribute to a much clearer picture. Near Γ the new spectra exhibit two distinct peaks at 1.8 and 1 eV. They disperse upward with increasing wavevector, with the deeper feature dispersing more rapidly, and eventually merge at $k = \pi/2$. Beyond the maximum, as expected, only the holon branch is observed. Its intensity is considerably reduced, probably because of cross section effects, related to the larger O 2p weight in the hybrid band in this part of the BZ. The enhanced visibility of the spinon and holon features enables a reliable analysis of the dispersion within the t–J model, which yields $J = 0.23$ eV and $t = 0.65$ eV, in good agreement with other experimental and theoretical estimates for this compound. The same spectral weight distribution is repeated essentially without change and following the lattice periodicity over a broad momentum range, providing a very useful redundancy of the data.

Attempts to reproduce the spectra between Γ and $k = \pi/2$ by two separate Gaussian line shapes at the holon and spinon positions, plus an integral background, yield a poor fit, with much spectral weight unaccounted for between the two peaks. This is also consistent with the continuum predicted between the holon and spinon singularities in an LL scenario. However, while t–J or infinite-U Hubbard model calculations provide a satisfactory qualitative description of the experimental data, the agreement is not quantitative. A further broadening of 0.45 eV for the holon and 0.65 eV for the spinon peak—which is well beyond the experimental resolution—is necessary to reproduce the data. The origin of the broad line shape, which is common to many oxides and appears to be largely intrinsic, is uncertain. Electron–phonon coupling is not included in the purely electronic models, but has been shown to have a strong effect on the spectra of CDW systems, and it may contribute to the large spectral width. This is an important and challenging issue, which calls for more theoretical investigations. It should be also noticed that the choice of photon energy, and possibly materials issues, may be more critical than expected. Soft x-ray ARPES data measured with the goal of reducing the contribution from the sample surface, have shown quantitative discrepancies with the data obtained at low and intermediate photon energies (Suga *et al* 2004). The higher-energy results take advantage of a much larger sensitivity to the Cu 3d states, but the dispersing feature is broad. A best fit of the k-dependent line shape with a 1D half-filled Hubbard model was achieved for $J = 0.2$ eV and $t = 0.4$ eV. More importantly, the spinon and holon branches could not be separated, a result which was then interpreted as reflecting an appreciable coupling between the two excitations.

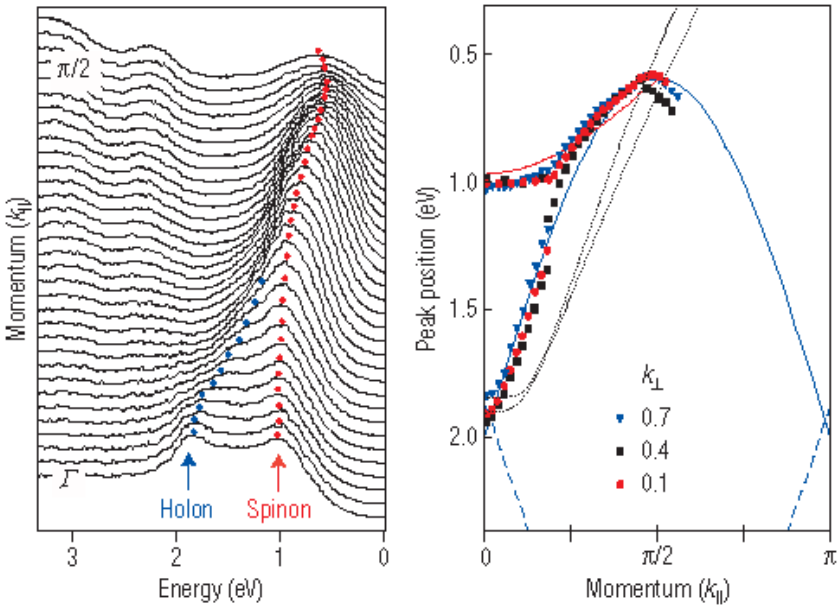

Figure 5. ARPES spectra (left; $h\nu = 85$ eV) of $SrCuO_2$ showing separate spinon and holon features, whose dispersion is reproduced in the right panel. Reprinted by permission from Macmillan Publishers Ltd: *Nature* Kim *et al* (2006), copyright 2006.

The influence of a slight hole doping on the electronic structure of a 1D insulator has been recently investigated in samples of $Sr_2CuO_{(3+d)}$ grown under oxygen pressure (Kidd *et al* 2008). Doping of course has a dramatic effect on 2D cuprates, where a small number of extra electrons or holes turns the AFM parent compounds into a high-T_c superconductor. The corresponding effect on the 1D cuprate is apparently weaker for an estimated doping level $d < 0.1$. At variance with a simple semiconductor scenario, the Fermi level does not shift to the top of the valence band, but remains in the gap. The Cu–O hybrid band shifts only slightly towards E_F, and the band maximum remains at $k = \pi/2$ within the experimental accuracy. All these observations may be the results of strong electronic correlations, but could also suggest that the actual doping level, which was not precisely determined, was lower than estimated. Nevertheless, the line shape is somewhat sharper than in the pristine compound, so that the spinon and holon peak positions could be determined even at the low photon energy (15.2 eV) utilized in the experiment. A separate fit of the dispersion within the t–J model yields $J = 0.26$ eV and $t = 0.82$ eV.

In metals, the occurrence of electron fractionalization has been strongly advocated for the Mo 'purple bronze' $Li_{0.9}Mo_6O_{17}$, whose 1D properties have been already discussed (Denlinger *et al* 1999, Gweon *et al* 2001, Allen 2002). What makes this compound particularly interesting in the search for non-FL behavior is the apparent lack of metal–non-metal instabilities down to very low temperatures, and the corresponding <1 meV experimental upper limit for any possible energy (pseudo)gap. The ARPES spectra (figure 6, left) do not exhibit the spinon and holon singularities expected for an LL, but rather a broad peak dispersing with wavevector, and a broad tail extending to E_F. However, the LL spectrum is considerably modified when interactions are very strong and long ranged. In this case the spinon edge singularity of the spectrum is strongly damped and only an abrupt onset, broadened by temperature and by the experimental resolution, is left in the spectra. This regime corresponds to large ($\alpha > 0.5$) values of the singularity index of the model. α is the non-universal exponent which appears in the asymptotic power-law expression for the density of states of the Luttinger model, and can be determined from momentum-integrated photoemission spectra. Such an analysis would yield $\alpha = 0.6$ for the purple bronze. However, α also enters the renormalization factor for the dispersion of the holon Fermi velocity (the spinon velocity is not renormalized). With a measured renormalization factor of 5, an even larger $\alpha = 0.9$ is required to match the dispersion in the ARPES spectra. The spectral line shape calculated for this value is shown in the right panel of figure 6. The spectra bear no direct spinon signature, but the energy position of the extrapolated leading edge is meaningful. The reasonable agreement between the experimental and calculated values of this quantity (shown in the insets) was taken as evidence supporting the LL case. A subsequent independent determination of the singularity index by scanning tunneling spectroscopy (STS) also yielded a large $\alpha = 0.6$ value, which is in agreement with the momentum-integrated PES data, but not with ARPES (Hager *et al* 2005). The issue has been recently revisited by a new analysis of temperature-dependent PES data in an LL scenario, which takes into account the two-band nature of the band structure of $Li_{0.9}Mo_6O_{17}$ around the Fermi surface (Wang *et al* 2006). This analysis, which goes beyond standard 1D theory, finds a strong temperature dependence of the parameters, and in particular a smooth transition from $\alpha = 0.9$ at RT to $\alpha \approx 0.6$ below 50 K, which can apparently reconcile the different experimental results.

2.4. Organic metals

Organic 1D materials, namely the Bechgaard salts $(TMTSF)X_2$ and $(TMTTF)X_2$, as well as TTF-TCNQ, have been a subject

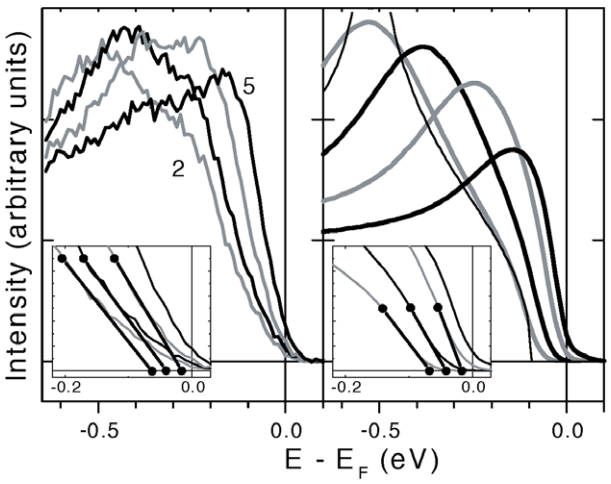

Figure 6. ARPES spectra of the 'purple bronze' $Li_{0.9}Mo_6O_{17}$ in the first half of the BZ (left) and calculated spectra in the Luttinger model (right). The insets highlight the high-energy onsets of the line shapes. Adapted from Denlinger *et al* (1999).

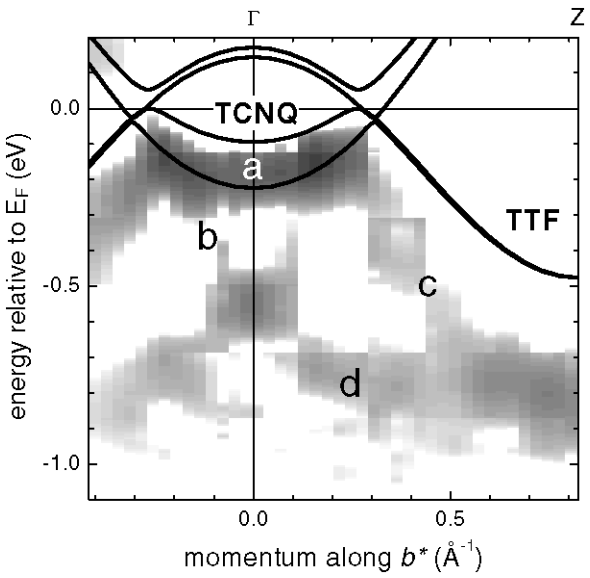

Figure 7. ARPES intensity map of TTF-TCNQ. Features 'a' and 'b' are interpreted as the spinon and holon associated with the TCNQ conduction band; 'd' belongs to the corresponding 'shadow band' predicted by the 1D Hubbard model; 'c' is the renormalized TTF conduction band. Reprinted with permission from Claessen *et al* (2002). Copyright 2002 by the American Physical Society.

of active research for more than three decades (for a recent review: (Dressel 2003)). Transport, magnetic and thermodynamic measurements have revealed clear signatures of non-FL behavior in these systems, and have been utilized to explore various characteristic 1D instabilities. The more recent interest for their spectroscopic properties has been initiated by the observation that ARPES spectra of these compounds lacked the usual QP features (Zwick *et al* 1997, 1998) and that the intensity was strongly reduced in the vicinity of the Fermi energy, in good analogy with the spectra of the inorganic 1D materials. The identification of possible spectral manifestations of truly 1D NFL behavior has been harder, even with the improved experimental conditions of the latest generation of ARPES experiments. In the insulating MX-chain compound $[Ni(chxn)_2Br]Br_2$ (chxn = 1R, 2R-cyclohexanediamine), for instance, a broad feature was observed to disperse in the chain direction from Γ to the band maximum at $\pi/2$, similar to the case of $SrCuO_2$ discussed above (Fujimori *et al* 2002). However, the other typical LL spectral features could not be detected, possibly as a result of the smaller charge-transfer energy gap $\Delta \approx 1$ eV in the organic compound.

TTF-TCNQ (tetrathiafulvalene tetracyanodimethane) provides a more compelling case for genuine 1D physics, not only at the meV scale of the low-energy excitations near the Fermi level, but also on a much larger energy scale. The electronic structure of this double-chain material is determined by the charge transfer between the donor TTF chain, built from stacked planar TTF molecules, and the acceptor TCNQ chain, built from a similar stack of TCNQ molecules. To satisfy the charge neutrality condition the TTF- and TCNQ-derived bands must therefore cross exactly at the Fermi surface, if small hybridization effects are neglected (figure 7). TTF-TCNQ is a metal at RT, and its strongly anisotropic conductivity sharply increases with reduced temperature, before a sudden drop at 54 K, where a CDW develops, at first on the TCNQ chains. Below 38 K the whole FS is removed and the material is an insulator. From the observation by x-ray diffraction of strong $4\,k_F$ fluctuations, which indicate a tendency towards charge localization, it is generally believed that electronic correlations are fairly strong on the TTF chains.

A new set of ARPES data (Claessen *et al* 2002, Sing *et al* 2003) confirms previous high-resolution ARPES results (Zwick *et al* 1998). Namely, it shows the two conduction bands (a and c in figure 7) crossing at the Fermi level, and identifies a nesting vector $q_{CDW} = 2k_F = 0.5\,\text{Å}^{-1}$, in good agreement with the diffraction data. Despite a qualitatively good agreement with theory, the occupied TTF bandwidth is twice as large as in state-of-the-art DFT band structure calculations, which are considered to be quantitatively predictive for this material. A change in the tilt angle of the molecules along the stack could lead to an increased bandwidth, and it was suggested that this might indeed happen at the free surface of the sample, which is probed by ARPES. This hypothesis however was recently dismissed by careful angle-dependent polarized x-ray absorption spectra, which are quite sensitive to the molecular orientation (Sing *et al* 2007). The discrepancy between the calculated bandwidth and the experiment appears now as intrinsic. Moreover, recent theoretical developments suggest that the inclusion of a long-range component of the Coulomb repulsion in standard 1D models for strong correlation, like the Hubbard model, can indeed yield an upward renormalization of the TTF bandwidth (Bulut *et al* 2006). Extending the range of the Coulomb interaction is also crucial to generate the large values of the α exponent, well beyond the $\alpha = 1/8$ limit of the standard Hubbard model. Such values are necessary to reproduce the peculiar ARPES line shapes, in particular the almost linear high-energy onset of the spectra.

The data of figure 7 also show very interesting features ('b' and 'd') which are not predicted by structure band

calculations. Within an LL scenario, feature 'b' is the holon branch corresponding to the spinon branch 'a' for the TCNQ band. Indeed, the measured dispersion can be reproduced by a model calculation with $t = 0.4$ eV and $U = 1.96$ eV, and a moderately strong coupling ratio $U/t \approx 5$. The high-energy feature 'd' also belongs to the holon branch, and it cannot be described by the Luttinger model, which is relevant at a much smaller energy scale. It is however naturally explained within the Hubbard model, which predicts a holon band symmetrically dispersing around $k = k_F$ and crossing the Fermi level at $-k_F$ and $+3k_F$. The data illustrate the dispersion down to its minimum at -0.8 eV at k_F, while the intensity of the 'shadow band' beyond k_F is below the detection limit. The Fermi level crossing of the TCNQ band at $+3k_F$, and the corresponding intrinsic $4k_F$ periodicity, were clearly observed in a later experiment (Ito *et al* 2005). The same data showed the straightening of the Fermi surface—or, more precisely, of the Luttinger surface (Dzyaloshinskii 2003)—leading to a good $2k_F$ nesting at low temperature.

Another interesting aspect of TTF-TCNQ is the temperature dependence of the spectral function (Zwick *et al* 1998, Claessen *et al* 2002). As already observed (Zwick *et al* 1998), the spectra show no intensity at E_F in the metallic phase. A careful normalization of the data shows also a continuous spectral weight transfer from the spinon to the holon branch with increasing temperature. This spectral weight transfer occurs on an energy scale which is much larger than k_B T. It is a genuine signature of (1D) correlations, which cannot be accounted for by conventional models, even including the effect of Peierls fluctuations. TTF-TCNQ appears therefore as one of the best actual realizations of the theoretical concepts underlying the electronic structure of 1D systems. Nonetheless, not all aspects of the problem are well understood, most notably the lack of evidence of spin–charge separation on the TTF band, where electronic correlations should be even stronger than within the TTF band. Clearly, a future comprehensive theory is required to reproduce the dissimilar spectral properties of the two coupled chains.

3. Quasi-1D systems at metal surfaces

Because of the short photoelectron mean free path, low-energy photoemission experiments are extremely sensitive to the very few topmost layers of a solid. ARPES is therefore ideally suited to the investigation of specially designed surfaces and interfaces, which may exhibit tailored electronic properties. Surface science has made impressive progress in the last 15 years in the fabrication of such artificial structures. In particular, exploiting self-organization processes at surfaces, it has been possible to demonstrate the fabrication of well ordered nanostructures and low-dimensional objects with a sharp size distribution (Brune *et al* 1998, Barth *et al* 2005, Li *et al* 2002, Didiot *et al* 2007, Kern *et al* 1991, Néel *et al* 2006). In this context, the choice of the substrate is an important degree of freedom. A specific substrate can be chosen for its specific band structure at the Fermi level, for its magnetic properties or again for the specific nature of the bonds (hydrogen, metallic or covalent) to the deposited materials. Therefore, surface science opens an extremely broad panel of artificial systems which can be studied in particular for their electronic properties. ARPES is very complementary to scanning tunneling microscopy and spectroscopy (STM and STS), as will be apparent in the following, where selected results on quasi-1D-systems grown on metallic and semiconductor substrates are described.

3.1. Self-organized anisotropic systems at metal surfaces

3.1.1. On the dimensionality of confined Shockley surface states. Noble metals exhibit Shockley surface states (Shockley 1939). These states derive from sp bands and behave as a quasi-2D electron gas on flat surfaces (Reinert *et al* 2001), i.e. they have a parabolic dispersion around $\bar{\Gamma}$ in the L projected band gap of the (111) faces. As predicted by Bychkov and Rashba (Bychkov and Rashba 1984), these 2D surface bands are split in wavevector by the spin–orbit (SO) interaction, as a result of the breakdown of inversion symmetry at the surface. Split bands have indeed been experimentally observed by ARPES for Au(111) (LaShell *et al* 1996), while the SO splitting at the Ag(111) and Cu(111) surfaces is too small for a direct observation (Cercellier *et al* 2004). Dense faces of transition metals, e.g. Ni(111), may also exhibit similar dispersive states (Pons *et al* 2003, Higashiguchi *et al* 2007), even if it is still unclear if they are true surface states or rather resonances, and to what extent they can be spin polarized.

On the pristine, flat surfaces, these states exhibit long lifetimes (Li *et al* 1998, Kliewer *et al* 2000). In particular, the electron–electron contribution is small, because (i) the surface density of the Shockley states is very low ($n_S \approx 7 \times 10^{-3}$ Å^{-2} for Cu(111)) and (ii) they are located in a gap of the projected bulk band structure, so that their interaction with bulk states tends to be weak. The electron–electron contribution to the lifetime scales as $(E - E_F)^{-2}$, in agreement with the ideal asymptotic Fermi liquid behavior near E_F (Burgi *et al* 1999, 2000, Vitali *et al* 2003, Crampin *et al* 2005). As far as ARPES is concerned, since the Shockley surface states are confined to the first atomic planes of the crystal, selection rules for the perpendicular wavevector k_z are considerably relaxed. Also, the contribution of the photoelectron's lifetime—as opposed to the 'intrinsic' hole lifetime—to the measured linewidth is minimal (Smith *et al* 1993). Finally, due to their high spectral density in the last planes of the crystal, Shockley states are very sensitive to surface defects such as step edges, deposited atoms, molecules or nanostructures.

STM studies have shown that the scattering of the Shockley surface states at step edges or point defects induces standing wave patterns (Crommie *et al* 1993a) of the electronic density and—if two defects are close enough—spatial confinement (Crommie *et al* 1993b). This suggests a strategy for producing 1D states at metal surfaces whereby electrons are confined between potentials related to strongly anisotropic structural architectures (Hörmandinger and Pendry 1994). These surfaces must exhibit a high regularity and long-range order for meaningful measurements of k-resolved electronic properties by a spatially averaging technique like ARPES. These conditions can actually be achieved in self-organized structures.

Shockley states of vicinal surfaces

One direct way to achieve 1D structural anisotropy at (111) surfaces is to use vicinal samples. They are produced by cutting a single crystal at a small angle with respect to the [111] high-symmetry plane in order to create a substrate which consists of flat terraces separated by atomic step edges. The repulsion between the step edges can induce a highly regular spacing of the steps. Therefore, the whole sample exhibits a periodic array of identical potential barriers—related to the step edges—for the Shockley surface states. The surface electronic states are perturbed, and hopefully localized, in the direction perpendicular to the steps, while they are only weakly affected in the parallel direction.

The quality of the metallic vicinal surfaces drastically depends on the Miller indices, i.e. on the average size of the terraces (Desjonquères *et al* 2002); namely, some surfaces are not stable and reorganize by faceting. Vicinal surfaces are quite sensitive to the surface preparation, crystal purity and the precision of the cutting angle. Often, the protocols for preparing flat noble metal surfaces for state-of-the-art high-resolution ARPES experiments, such as presented in (Reinert *et al* 2001), may be extended to the case of vicinal surfaces. Moreover, thermal fluctuations of the step edges may induce—even at RT, depending on the material and the Miller indices of the surface—a broadening of the size (d) dispersion of the terraces. The latter is clearly a very important parameter affecting the quality of the ARPES results.

Au(111) and Cu(111) vicinal surfaces have been extensively studied by ARPES and STM/STS. Photoemission experiments have shown that, depending on the terrace size, the surface presents superlattice states (SLSs) or quantum well states (QWSs) perpendicular to the step edges. The latter case corresponds to the asymptotic behavior of independent terraces, where the electronic states are strongly confined by the step-induced potential. This confinement leads to quantized wavevectors $k_\perp$ and to discrete energy levels E_n, at $k_\parallel = 0$. Ideally, the ARPES intensity $I(E, k_\perp)$ should be different from zero only at discrete pairs of points $(E_n, \pm k_{\perp,n})$, corresponding to the eigenlevels of the perpendicular resonator. In reality, all the experimental ARPES spectra measured along the perpendicular direction show a parabolic background on top of which are superimposed peaks due to confinement. This observation has been attributed to the smearing of the peaks due to the size dispersion $\sigma(d)$ of the terraces (Baumberger *et al* 2004a). Parallel to the step edges, if no additional scattering potential is introduced, the $E_n(k_\parallel)$ dispersion of each sub-band n is continuous and parabolic. Only the first eigenstate $n = 1$ has a significant spectral weight at normal emission and is observed by ARPES (Mugarza *et al* 2002, Didiot *et al* 2006, Malterre *et al* 2007). SLSs correspond to the ideal situation where all terraces are coherently coupled to each other. In this case, no energy quantization is observed. If the structural properties are homogeneous, the dispersion reflects the periodicity of the potential probed by the surface states.

The transition from 1D states to 2D states as a function of the terrace size has been studied on gold vicinal surfaces with different Miller indices (Ortega *et al* 2000, 2002, Mugarza *et al* 2002, Mugarza and Ortega 2003, Mugarza *et al* 2003). The Au(322) surface shows a broad line shape, and a parabolic dispersion with $k_\perp$, compatible with SLSs. The dispersion is on the other hand negligible for Au(788), which marks the crossover between the SLS and the QWS case (figure 8). For Au(23 23 21) the spectra (not shown) exhibit sharp non-dispersive features separated by gaps, which can be described in terms of discrete 1D QWSs. The analysis of the data with a Kronig–Penney (KP) model implies a reduced step potential, i.e. a less efficient confinement, for the smaller terrace sizes. It was attributed to a progressive shift of the surface band out of the projected band gap. The resulting increased coupling with the bulk states reduces the confining effect of the step edges on the Shockley states, and can therefore explain the QWS to SLS transition.

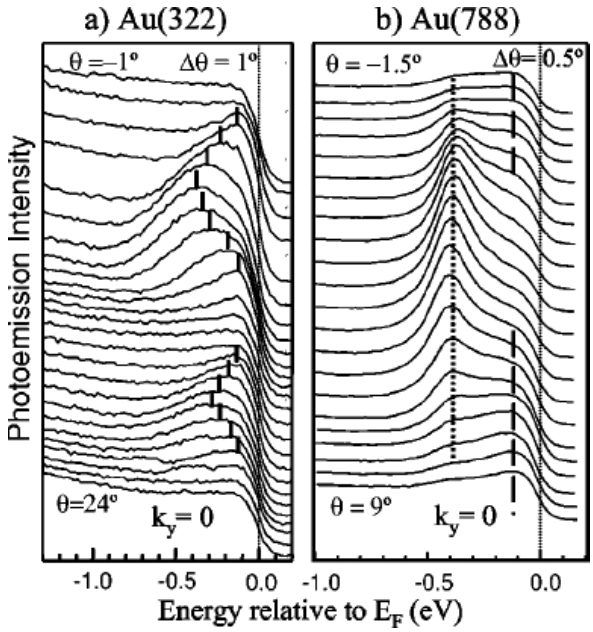

Figure 8. Dispersion in the direction perpendicular to the step edges of (a) SLSs at Au(322), $d = 12$ Å (the parabolic dispersion is duplicated due to umklapp by the wavevector of the step periodicity), and (b) QWS at Au(788), $d = 39$ Å. Adapted from Ortega *et al* (2002).

A similar transition was also demonstrated by ARPES at Cu(111) vicinal surfaces for terraces between $d = 17$ and 20 Å (Ortega *et al* 2000, 2005, Baumberger *et al* 2004a). STS data on this system illustrate the superposition of the effect of the superlattice, and of signatures of localized states (Sánchez *et al* 1995, Hansmann *et al* 2003). *Ab initio* calculations showed that the KP model, generally used to analyze the STS and ARPES data (Sánchez *et al* 1995, Ortega *et al* 2000), overestimates the energy gaps in the band structure. They did confirm the large variation of the step potential with the terrace size, and interpret the occurrence of a minimum of the barrier strength for 18 Å as an evidence for the transition (Ignatiev *et al* 2007). The surface-to-bulk delocalization mechanism for the transition has been questioned by data which did not show any significant change in the evanescent behavior of the surface states along the bulk direction for the case of the Cu(443) SLS with respect to the Cu(665) QWS (Baumberger *et al* 2004a).

On the other hand, the SLS to QWS transition follows a sharp variation of the surface state lifetime. This is consistent with the fact that, at variance with the SLS, the QWS can only scatter with bulk states at the step edges.

In spite of their low density, the contribution of the surface states to the surface total energy may play a crucial role in the stability of copper vicinal surfaces (Baumberger *et al* 2004b). Indeed, Friedel oscillations of the surface charge density mediate a long-range interaction between scatterers like the step edges (Lau and Kohn 1978). In a different context, an interplay between surface electronic states and surface structure is at the origin of the stabilization of superlattices of Ce atoms on Ag(111) (Silly *et al* 2004). For Cu(443)—with an average terrace width of ≈16 Å—a full energy gap of ≈450 meV around E_F in the SLS band dispersion has been attributed to the interaction between the structural array of steps and the electron gas (Baumberger *et al* 2004b). The gapped band structure, which exhibits a van Hove singularity below the Fermi level, causes a reduction of the electron total energy of ≈10 meV per unit cell in this system with respect to a non-stepped surface.

Further experiments (Shiraki *et al* 2004, Baumberger *et al* 2002, Schiller *et al* 2005, Didiot *et al* 2007) have shown that the step potential can be modified by attaching rows of atoms, molecules or nanostructures to the step edges. The change in the step edge configuration can then trigger an SLS to QWS transition. It has also been proposed that Fe rows deposited at step edges of Cu(111) vicinal surfaces would induce spin-polarized surface states (Ignatiev *et al* 2007). Remarkably, 1D rows of atoms grown at vicinal step edges were shown to exhibit unexpected long-range ferromagnetic order due to a substrate-induced magnetic anisotropy (Gambardella *et al* 2002).

It is somewhat surprising that the dispersion in the direction parallel to the steps, i.e. the 1D propagation direction, has not been extensively studied so far. ARPES measurements have been performed on the SO-split Shockley states at Au(111) vicinal surfaces. These surfaces exhibit an additional periodicity along the parallel direction, which derives from the herringbone reconstruction of the flat surface (Barth *et al* 1990). It consists of an alternation of fcc and hcp domains separated by stacking faults. In this case, the SO-split nearly-free-electron band doublet is perturbed by the superlattice potential, leading to band folding and the opening of spin-selective gaps (Didiot *et al* 2006, 2007, Malterre *et al* 2007).

Oxide stripes at Cu(110)

Among the 1D architectures obtained at surfaces by self-organized growth, the elegant case of the O/Cu(110) interface is noteworthy (Kern *et al* 1991). This system has been studied as a template for further growth and for its electronic properties. The Cu(110) surface exhibits a Shockley surface state at the $\bar{Y}$ point of the surface Brillouin zone of the (1 × 1) non-reconstructed surface. Oxygen adsorption leads to the formation of homogeneous, periodic stripes of (2 × 1) reconstructed Cu–O domains, in the so-called added-row structure. These stripes are elongated in the [001] 'parallel' direction. The width and the periodicity of the stripes along the direction perpendicular to the $(\text{Cu chain})_n$–$(\text{CuO chain})_m$ rows are determined by the oxygen coverage ($\theta < 0.5$ ML). It has been shown that the stripes induce a confinement of the Shockley surface state of the uncovered Cu surface.

The width of the oxide stripes is small for low O coverage. Thus, the interactions between the uncovered adjacent stripes through the narrow oxide stripes can be described with a KP model in the perpendicular direction (Bertel and Lehmann 1998) at RT. However, at low temperature, thermal excitations are not strong enough with respect to the potential barrier to allow coupling of the electronic states through the oxide stripes. The clean copper stripes are uncoupled even at RT when the width of the oxide domains is large. In both cases, the Cu stripes behave as a collection of independent quantum wells (Berge *et al* 2004, Nagira *et al* 2007a, 2007b). This crossover form coupled to non-coupled stripes has been described as a coherent to incoherent transition (Berge *et al* 2004). Correlation effects are weak in this system, probably mainly as a result of the low electron density at the surface (Menzel *et al* 2005).

3.1.2. Tamm states at anisotropic surfaces: Pt(110), H/Pt(110) and halogen chains at the Pt(110) surface. Correlation effects are important in platinum, which is indeed believed to be on the verge of ferromagnetism. The Pt(110) surface exhibits the (1 × 2) so-called missing-row reconstruction, which presents a clear 1D anisotropy (figure 9(a)). Clean and Br-or H-covered Pt(110) surfaces exhibit Tamm states (TSs) at the Fermi level. These states of d symmetry are—in this particular case—resonant with bulk states. They exhibit a high density of states and a weak dispersion parallel to the surface. This, and the surface anisotropy, enhances the hybridization along the chain (parallel) direction of the missing-row reconstruction of the substrate, and reduces it in the [001] (perpendicular) direction. As a result, the clean and the Br- and H-covered Pt(110) surfaces are interesting examples of quasi-1D systems. In particular, the line shapes of the TS have been investigated, as indicators of the interplay of electronic correlations and low dimensionality (Minca *et al* 2007). The H-covered phase was simply obtained by exposing the substrate to the residual gas (mostly composed of H_2) of the UHV chamber (Menzel *et al* 2006, 2005). The structure of the H-covered Pt(110) is supposed to be the same as that of the clean substrate. Br was deposited on the surface with a solid-state electrolysis cell (Deisl *et al* 2004, Menzel *et al* 2005). The resulting c(2 × 2) structure is presented in figure 9(b).

Two surface resonance bands along the $\bar{Y}\bar{S}$ and $\bar{S}\bar{X}$ directions meet at a saddle point at $\bar{S}$ and at $E = E_F$ for the three systems. This saddle point is associated with a strong spectral weight. In figure 10, a quasi-linear evolution of the spectral weight of the QP peak with temperature is observed for the c(2 × 2) Br/Pt(110) surface. This observation has been attributed to a second-order coherent to incoherent transition from coupled to uncoupled chains when the temperature is of the order of the lateral coupling energy (Menzel *et al* 2005, Minca *et al* 2007). For H/Pt(110), the temperature dependence of the spectral weight was measured at the $\bar{X}$ point, which is

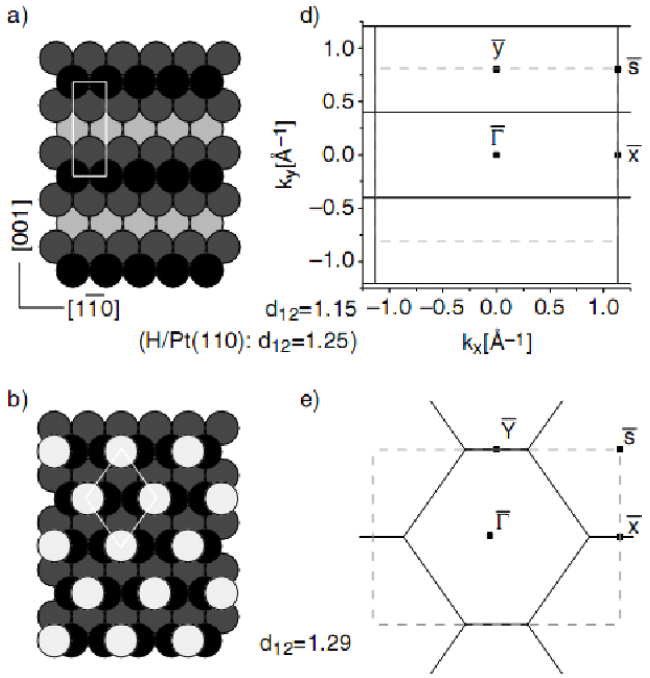

Figure 9. (a) Real space missing-row structure and (c) surface BZ (SBZ) of the clean (1 × 2) reconstructed Pt(110) substrate. (b) Real space structure and (e) SBZ of the c(2 × 2) Br/Pt(110) system. H/Pt(110) is supposed to have the same structure as Pt(110), but where H occupies the short bridge sites between the Pt atoms. The dashed lines are related to the 1 × 1 surface Brillouin zone (SBZ). Adapted from Menzel *et al* (2005).

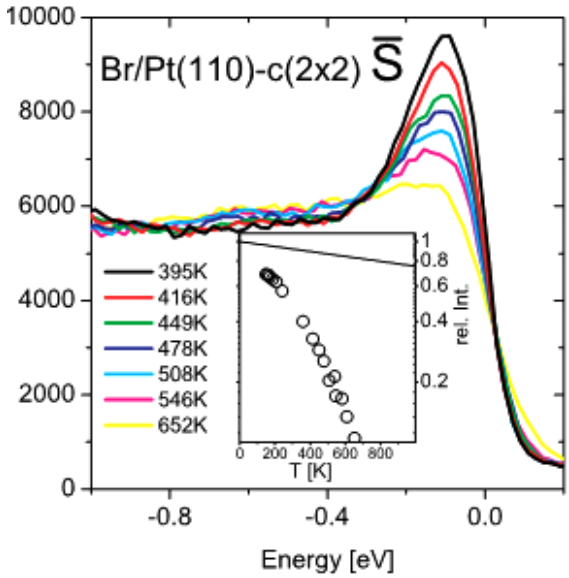

Figure 10. Temperature evolution of the photoemission intensity at $\bar{S}$ for c (2 × 2) Br/Pt(110). The inset is a plot of the integrated QP intensity. Adapted from Minca *et al* (2007).

equivalent to the $\bar{S}$ point of the (1 × 2) reconstructed surface. H adsorption increases the overlap of the bulk and the resonance states, and favors the formation of a coherent 2D surface resonance (Menzel *et al* 2006, 2007). Finally, for Br/Pt(110) c(2 × 2), an analogy has been drawn between the evolution with temperature of the QP spectral weight at E_F, and that of the well known *peak–dip–hump* ARPES feature of the high-T_c cuprates (Menzel *et al* 2005).

3.1.3. Other quasi-1D systems at metal surfaces.

Au on Ni(110). ARPES measurements of Au chains grown at the Ni(110) surface have evidenced a strong dispersion along the chains and an absence of dispersion perpendicular to the chains in agreement with *ab initio* calculations. Remarkably, the data suggest that confinement within the chain structure depends on the electron spin (Pampuch *et al* 2000).

Tungsten carbide. ARPES experiments have demonstrated the lateral quantization and a quasi-1D character of the electronic states of the R(15 × 3) reconstruction of C/W(110). This substrate has been utilized as a template for growing Au atomic wires, which showed a similar 1D behavior (Varykhalov *et al* 2005, Varykhalov and Gudat 2005).

Chains of adatoms fabricated with an STM tip. STM has been used for the fabrication of chains of a few atoms on metallic substrates (Nilius *et al* 2002, Fölsch *et al* 2004) and on thin oxide layers (Kulawik *et al* 2006). The electronic structures of 2D and 1D silver clusters on Ag(111) have been recently compared (Sperl *et al* 2008). In general, while STS data suggest a quasi-1D behavior of the states close to the Fermi level, these 1D nanostructures have not yet been studied by ARPES.

Anisotropic molecular systems. Anisotropic molecular systems have been obtained both on flat and vicinal metal surfaces. STM/STS results indicate that self-assembled supramolecular chains grown on Ag(111) confine the surface states of the substrate and produce 1D-like resonators (Pennec *et al* 2007). The quasi-1D character of the electronic states of single molecular rows of C_{60} molecules occupying the terraces of Cu(553) has been shown by ARPES (Tamai *et al* 2006). The deposition of TTF-TCNQ on Au(111) leads to the formation of two interface bands with hybrid molecular and metal character, for which STS reveals a quasi-1D metallic free-electron-like dispersion (Gonzalez-Lakunza *et al* 2008).

4. Self-assembled atomic chains at silicon surfaces

Numerous studies have been performed on self-assembled atomic chains on silicon single-crystal surfaces. Under appropriate conditions, the deposited metal atoms spontaneously self-assemble in chain structures. They are tightly bound to the substrate by back-bond states, which are well removed from the Fermi energy, and therefore probably irrelevant for the low-energy electronic properties of the system. On the other hand, the states near E_F which may exhibit the exotic 1D electronic properties lie—in part or entirely—in a projected bandgap, and are relatively free from the influence of the substrate. ARPES studies of atomic wires have often been complemented by STM and STS measurements to gain information on the local structure of the chains, which very often plays a major role. The

electronic quasi-1D nature of these artificial systems is revealed by the very small dispersion of their surface states in the direction perpendicular to the chains. The interchain coupling can be tuned to some extent by varying the structural and physical parameters of the interface.

4.1. Au chains on flat and stepped Si(111) surfaces

Si(111)(5 × 2)–Au: a metal-to-semiconductor transition by doping

1D atomic wires have been initially fabricated and studied by ARPES at the Au–Si(111) interface, where a (5 × 2) structure with three equivalent domains forms for an optimum Au coverage of ≈0.4 ML. A small intentional miscut (1°–2°) breaks the threefold degeneracy and favors the nucleation of a single domain, where Au chains run parallel to the surface steps. A metallic surface state (S_1) was reported to cross E_F along, but not perpendicular to, the chains (Collins *et al* 1995). It was considered as the first evidence of photoemission spectral intensity at the Fermi level from a quasi-1D system. This observation was later confirmed by ARPES (Okuda *et al* 1997b) but not by inverse photoemission (IPES) (Hill and McLean 1997b). Subsequent ARPES data have suggested the occurrence of a Peierls transition in this system (Losio *et al* 2000), based on the properties of a sharp adatom-derived band (S_2). This band disperses to a maximum at the zone boundary of the (5 × 2) SBZ, and the energy gap was interpreted as a Peierls gap, associated with the doubled periodicity along the chains. The Peierls scenario was soon revisited when a clear E_F crossing of state (S_1) was observed in the second BZ, and S_2 was seen to exhibit a pseudogap rather than a true gap (Altmann *et al* 2001). Interestingly, a clear change of dimensionality is observed between the top and the bottom of the S_2 band (Losio *et al* 2000, Himpsel *et al* 2002). Its dispersion is 1D-like close to the Fermi level and it gradually becomes more 2D-like at larger binding energy. More recent data have confirmed the intrinsic character of the S_1 feature, but measured a ≈0.2 eV bandgap (Matsuda *et al* 2003).

ARPES (McChesney *et al* 2004) and STM experiments (Yoon *et al* 2004) have been performed to clarify the conflicting results on the S_1 band. A change from metallic to semiconducting character has been observed when additional Si adatoms are located on top of the chains. A Si-rich surface leads to a phase separation into metallic (5 × 2) chains without Si atoms, and semiconducting subsections with an adatom-induced (5 × 4) superlattice. Two different kinds of S_1 bands were then identified. A first, metallic (S_1'), band, assigned to the metallic parts of the surface, crosses E_F at the boundary of the (5 × 4) surface BZ. A second, semiconducting (S_1''), band, corresponding to the semiconducting chain segments with Si adatoms, is backfolded at the zone boundary. Very recent ARPES results illustrate the metal-to-semiconductor transition induced by the deposition of Si atoms (Choi *et al* 2008). They confirm that at the minimum adatom density (36.8%) the electronic transport along the wires is controlled by the partially filled valence band S_1' (labeled S_2 in this reference), with a filling factor intermediate between 1/4 and 1/3. This band gradually shifts away from E_F with increasing adatom density and the bandgap increases linearly from 0 to ≈0.3 eV (figure 11).

Si(557)–Au: spin–charge separation versus Rashba spin–orbit splitting

Much ARPES work has been performed on uniform monodomain interfaces with a regular step structure. Unlike the case of a flat substrate, the length of 1D chains grown on vicinal Si(111) surfaces is not limited by the domain size of the reconstruction. Moreover, the atomic steps become a natural part of the reconstruction, and the resulting structures exhibit a strong 1D character, with essentially no dispersion perpendicular to the steps. Si surfaces tilted from the [111] direction, towards either $[\bar{1}\bar{1}2]$ or $[11\bar{2}]$, form a series of (111) terraces and stable step structures (Jalochowski *et al* 1997, Crain *et al* 2004). Regular arrays of 1D chains form parallel to the steps after the deposition of the optimum Au coverage. Various interfaces between Au and vicinal Si(111) surfaces have been investigated with the goal of tuning the band dimensionality and band filling (Crain *et al* 2004).

The Si(557)–Au system has been thoroughly studied by ARPES. The substrate has a miscut of 9.5° from [111] towards the $[\bar{1}\bar{1}2]$ direction, and an optimum Au coverage of 0.18 ± 0.04 ML yields one Au chain per unit cell (Crain *et al* 2004). Interest in this system was boosted by the observation of a 1D metallic band with vanishing spectral intensity at E_F, and no signatures of a temperature-induced transition. The ARPES spectra were split into two separately dispersing features, which apparently merged at k_F, as expected for spin–charge separation in 1D (Segovia *et al* 1999). Later data, however, (Altmann *et al* 2001, Losio *et al* 2001) have shown that the two spectral features are not degenerate at E_F (see figure 12), and therefore cannot be considered as the spinon and holon signatures in an LL scenario (Voit 1993). They are instead attributed to two closely spaced bands, one slightly more and the other slightly less than half-filled. They originate from degenerate or nearly degenerate electron levels: either from the same orbital and two chains within the unit cell, or from one chain with two orbitals per atom. A two-band scenario resolves the apparent contradiction between the metallic character of the interface, and an even number of electrons per unit cell. Temperature-dependent measurements of the spectral intensity at E_F suggest that the two bands undergo Peierls transitions with different critical temperatures. The slightly more than half-filled band gradually develops a gap at 120–270 K, while the transition for the second band is believed to occur above RT. This hypothesis is supported by the observation of a 2× modulation in STM measurements. The metallic band of the doublet was primarily assigned to the Si atoms at the terrace edge, while the gapped state was assigned to Si adatom chains within the terrace (Ahn *et al* 2003b, Yeom *et al* 2005). Another ARPES study (Crain *et al* 2004) did not report any backfolding or gap opening.

The two-band scenario is in conflict with first-principles DFT calculations, which suggest a qualitatively different picture (Sánchez-Portal *et al* 2004). The doublet is attributed to a single surface band, split in momentum (and energy) by

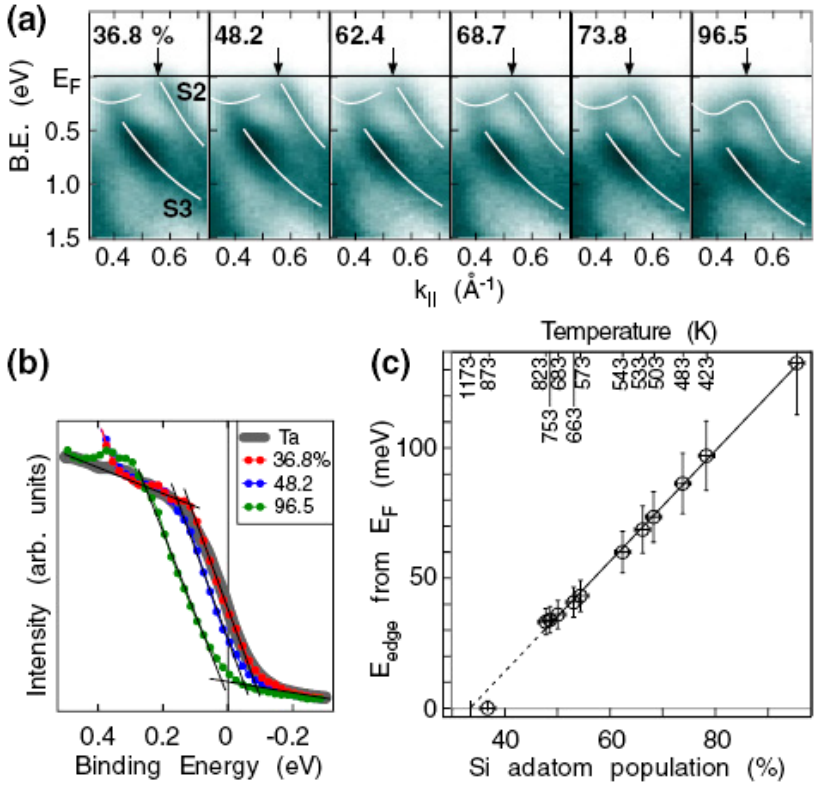

Figure 11. (a) Evolution of the band structure of Au atomic wires on Si(111) with increasing density of Si adatoms. The data were taken near E_F along the wires. (b) ARPES spectra for selected adatom densities and for a metal reference showing the evolution of the bandgap, which is summarized in (c). Reprinted with permission from Choi *et al* (2008). Copyright 2008 by the American Physical Society.

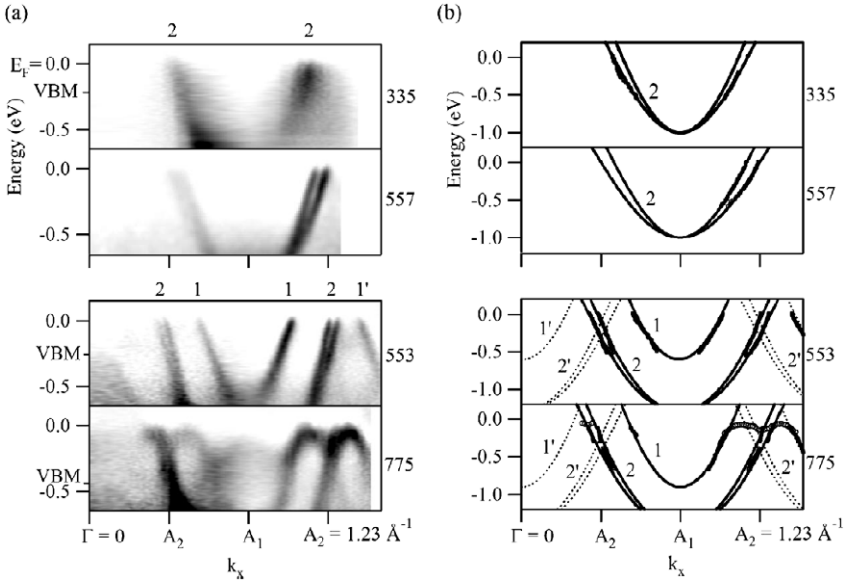

Figure 12. Band dispersions in the chain direction for various Au-induced 1D structures on stepped Si(111): Si(335)–Au, Si(557)–Au, Si(553)–Au and Si(775)–Au. The upper pair exhibits a doublet of nearly half-filled bands, the lower pair an additional fractionally filled band. The bottom of all bands lies at the 1D Brillouin zone boundary. Backfolded bands are indicated by dotted lines and primed labels. Reprinted with permission from Crain *et al* (2004). Copyright 2004 by the American Physical Society.

the combined effect of the spin–orbit interaction and of the lack of inversion symmetry at the surface. As mentioned in section 3.1, a similar splitting has been observed for the Shockley surface state at the Au(111) surface. This 'Rashba' scenario has been now convincingly established by a thorough analysis of recent high-resolution ARPES data (Barke *et al* 2006). These data clearly show that the doublet and its replica from the second BZ give rise to avoided crossings that are

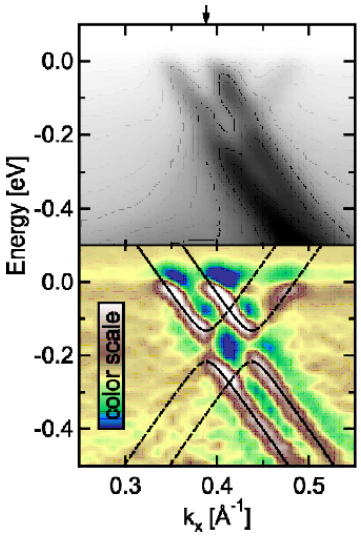

Figure 13. Raw (top) and high-pass filtered (bottom) ARPES map of Si(557)–Au at the band crossings near the 2×1 zone boundary. The avoided band crossings are offset horizontally, as predicted by the 'Rashba' scenario. Reprinted with permission from Barke *et al* (2006). Copyright 2006 by the American Physical Society.

symmetrically located around the BZ boundary, as required for a single SO-split band (see figure 13).

Si(553)–Au: uncorrelated CDWs on neighboring chains

The miscut angle for the Si(553) surface is 12.3° towards the $[11\bar{2}]$ azimuth. The optimum Au coverage of 0.24 ± 0.04 ML results in a single gold chain per unit cell, with ordered vacancies yielding an overall (1×3) periodicity. The ARPES band structure (see figure 12) exhibits a doublet similar to Si(557)–Au, and an additional band with a fractional filling, slightly larger than 1/4. All three 1D bands are assigned to rows of Si broken bonds. Backfolding of these bands is observed following the superlattice periodicity along the chains (Crain *et al* 2003, 2004). The estimated overall filling is 4/3, i.e. 8/3 electrons per (1×1) unit cell. It may be the result of doping by additional extra Si atoms, two per (1×3) cell, attached to the step edges. Such non-integer (and $\neq 1/2$) filling factor is interesting, because a similar chain would retain its metallic character even for rather strong electronic correlations. It should then be possible to investigate strong correlation effects in a metallic 1D systems if a similar structure could be created at the hexagonal SiC(0001) surface, where U is believed to be larger: $U \approx 2$ eV versus $U \approx 0.1$ eV for clean Si(111)(7×7).

Temperature-dependent LEED, STM and ARPES studies (Ahn *et al* 2005) concluded that two CDWs—with associated periodic lattice distortions (PLDs)—of $\times 3$ and $\times 2$ periodicities are simultaneously present on different atomic chains. Moreover, ARPES measurements showed that an energy gap opens for both the $\approx 1/4$-filled and one of the two 1/2-filled bands. The other 1/2-filled band is already gapped at RT, as for Si(557)–Au. The present understanding is that two different commensurate PLDs co-exist on neighboring atomic chains

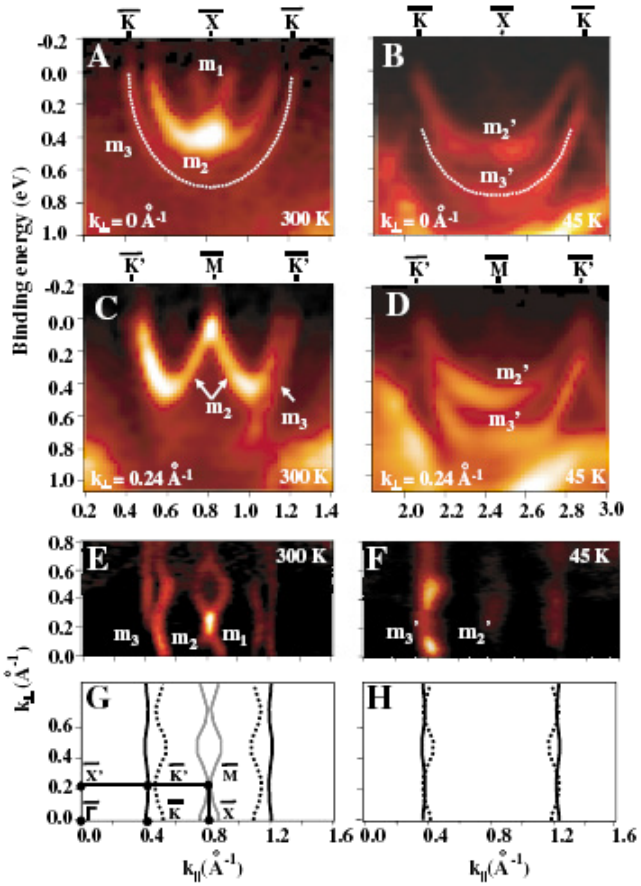

Figure 14. Measured energy bands of Si(111)–In along the wires ($k_{\parallel}$) in the metallic (RT) state at $k_{\perp} = 0$ (a) and 0.24 Å^{-1} (c) and in the insulating state (45 K) (b), (d). Constant energy maps at $E = 0$ for the metallic (e) and at $E = 0.1$ eV for the insulating phase (f) are schematically reproduced in (g) and (h), respectively. Reprinted with permission from Ahn *et al* (2004a). Copyright 2004 by the American Physical Society.

within an ≈ 1.5 nm-wide unit cell. The two adjacent PLDs are not spatially correlated and have different transition temperatures. The true ground state of Si(553)–Au should be not a metallic 1D non-FL, but rather an insulating broken-symmetry state. Temperature-dependent STM/STS results (Snijders *et al* 2006) suggest that the system first undergoes a Peierls distortion with doubled periodicity along the chains, while a defect-mediated CDW yields a $\times 3$ periodicity at lower temperature.

Si(335)–Au: decreasing the interchain spacing

The miscut angle of this surface is 14.4° from the [111] towards the $[\bar{1}\bar{1}2]$ direction, and an optimum coverage of 0.27 ± 0.04 ML results in a single Au chain per unit cell. The doublet of half-filled bands, with minima at the boundary of the surface BZ, is again present (see figure 12) (Crain *et al* 2004). However, there is no additional fractionally filled band, which is apparently only present on surfaces tilted towards $[11\bar{2}]$. The deviation from ideal 1D straight Fermi surface sheets is larger than for the other structures, due to the smaller interchain spacing (larger transverse interaction).

The estimated overall band filling is 0.8, or 1.62 electrons per unit cell, which can be compared e.g. with the corresponding value of 1.82 electrons for Si(557)–Au. This shows a clear correlation between the density of defects—which is larger for Si(335)—and the deviation from an integer (2) number of electrons, supporting the idea that defects act as dopants for the metallic chains.

Si(775)–Au

This surface is tilted by 8.5° from the [111] towards the [11$\bar{2}$] direction, and an optimum Au coverage of 0.25 ± 0.07 ML yields two Au chains per unit cell. ARPES shows an upper ≈1/4-filled band and a pair of lower 1/2-filled bands just like Si(553)–Au (Crain *et al* 2004). Si(775)–Au exhibits two clear similarities with the Si(111)(5 × 2)–Au interface: (i) both structures contain two Au chains per unit cell, and (ii) both present flat bands near E_F and a semimetallic character (figure 12).

Other Au-induced 1D structures on stepped Si surfaces with (111) facets

Si(995)–Au and Si(13 13 7)–Au have many similarities to the Si(553)–Au surface. Both of them are produced by a miscut from the [111] towards the [11$\bar{2}$] direction and exhibit a single Au chain per unit cell. Their unit cells probably have the Si(553)–Au structure as a subunit plus areas of uncovered silicon. Their electronic structures are therefore very similar to that of Si(553)–Au, with a ≈1/4-filled band and a 1/2-filled doublet (Crain *et al* 2004).

4.2. Au chains on different silicon surfaces

Si(5 5 12)–Au: an irreversible insulator-to-metal transition

Unlike the Si surfaces considered so far, which exhibit a regular array of steps and (111) terraces, the bulk-terminated Si(5 5 12) surface reconstructs in order to reduce its surface energy. The clean reconstructed surface has a unit cell consisting of two (337) and one (225) facets (Baski *et al* 1995). Au deposition leads, with increasing coverage, to the formation of various Au-induced facets, namely twofold (337), (5 5 11) and (225) facets.

The formation of two well ordered chain-like facets with different interchain distances—30.2 Å and 22.8 Å respectively for 0.15 and 0.5 ML coverages—has been reported (Lee *et al* 2002). ARPES has revealed two 1D surface states with identical dispersions along the chains. The shallower band has a metallic character and crosses E_F halfway between $\overline{\Gamma}$ and the surface BZ boundary. Later studies confirmed the formation of a well ordered nanowire array at Au coverages of 0.1–0.2 ML, but revealed a semiconducting surface (Ahn *et al* 2002b). This discrepancy results from an irreversible insulator-to-metal transition at 400–500 °C (Ahn *et al* 2003a). Since the change of the surface structure is not as abrupt as the change of the electronic structure, it has been suggested that the insulator-to-metal transition is not directly related to the formation of the facets. It may follow the rearrangement of the Au atoms and the formation of new Au chains on the surface. It was later shown that the initially reported metallic surface state is actually a doublet of closely spaced bands which are split at E_F. These bands are half filled and their behavior is very similar to that of the Si(557)–Au doublet. The similarities between the two systems are confirmed by STM atomic structure measurements (Ahn *et al* 2004b).

Si(110)(5 × 2)–Au

Although Si(110) is a low-index surface, it exhibits a strong tendency towards faceting. STM studies (An *et al* 2000, Röttger *et al* 2001) have shown a prevailing (16 × 2) surface reconstruction, together with smaller areas of (5 × 1) periodicity. The surface orders and flattens with the deposition of Au, and several reconstructions may develop, depending on the Au coverage and on the annealing parameters (Ino 1987). The 1D (5 × 2) reconstruction formed after deposition of 0.26 ML Au exhibits a doublet of bands with a metallic character (McChesney *et al* 2005), similar to the Si(557)–Au doublet, albeit with a larger splitting. This similarity suggests that also for the Si(110)(5×2) interface the elementary building blocks are steps and one gold chain incorporated into a Si(111) facet.

4.3. Other metals on Si(111)

Si(111)(3 × 1)/(6 × 1)–Ag

The formation of 1D nanostructures can be induced by the deposition of Ag on flat Si(111) substrates. Namely, annealing of the Si(111)($\sqrt{3} \times \sqrt{3}$)–Ag surface at ≈600 °C yields a 1D reconstruction with a (3 × 1) periodicity, which converts into (6 × 1) after cooling to RT (Gotoh and Ino 1978, Wilson and Chiang 1987). The structural properties of these 1D Ag-induced reconstructions have been thoroughly investigated (Gotoh and Ino 1978, Ichikawa and Ino 1980, Wan *et al* 1992, Weitering *et al* 1994). ARPES measurements on three-domain samples suggest that the stable structure has a c(12×2) symmetry, and that the (6 × 1) structure, which is stabilized at RT, is due to thermally induced disorder (Sakamoto *et al* 2001). Five relatively flat surface states have been observed, but no Fermi level crossing. The semiconducting nature of the surface agrees with STM/STS results, which found a bandgap of 0.9 eV (Carpinelli and Weitering 1996). A different set of ARPES data on a single-domain sample confirmed these results (Gurnett *et al* 2002). It showed nonetheless a significantly larger dispersion, and very good agreement with theoretical studies (Erwin and Weitering 1998, Kang *et al* 1998).

Si(111)(3 × 1)–alkali metals: a 1D Mott–Hubbard insulator

Alkali-induced quasi-1D (3 × 1) reconstructions have been observed after the deposition of 1/3 ML of K, Na or Li on clean Si(111)(7 × 7) surfaces at high temperatures (≈400°–600 °C) (Sakamoto *et al* 1994, Weitering *et al* 1996). By contrast, alkali-metal deposition at RT yields the so-called δ (7 × 7) reconstruction (Daimon and Ino 1985). In all proposed

structural models of the interfaces the alkali-metal atoms form chains—one chain per unit cell—which are separated by Si chains (Wan *et al* 1992, Okuda *et al* 1994, Erwin 1995, ong and Kang 1995). Synchrotron radiation ARPES data from three-domain samples have established the quasi-1D character of the surface states, and their semiconducting nature (Sakamoto *et al* 1994, Okuda *et al* 1997c, 1997a, Weitering *et al* 1996), in agreement with an earlier STM study (Jeong and Kang 1996). ARPES results on single-domain Si(111)(3 × 1)–Li surfaces revealed a pronounced surface state whose dispersion matches the calculated dispersion for the realistic honeycomb-chain-channel (HCC) model (Bromberger *et al* 2003). Deposition of excess Na adatoms on the 1/3 ML Si(111)(3 × 1)–Na surface induces the formation of a new well ordered (3 × 1) phase at a coverage of 2/3 ML. This so-called 're-entrant' Si(111)(3 × 1)–Na surface has been investigated by STM, HREELS and photoemission (Ahn *et al* 2002a). Interestingly it has been found to be a quasi-1D Mott–Hubbard insulator with $U = 0.8$ eV and $t \leqslant 0.1$ eV. This conclusion contrasts with a previous HREELS study (Lee and Chung 1998), which proposed a bipolaronic insulator. It should be noted that the simple Si(111)(3 × 1)–alkali-metal structure at 1/3 ML is a simple band insulator.

Si(111)(4 × 1)–In: a novel gap opening mechanism

The deposition of 0.9–1.2 ML of indium onto a Si(111) 7 × 7 substrate yields a (4 × 1) structure, composed of 1.3 nm wide 1D atomic wires. Each wire consists of an array of four parallel In chains between two Si chains (Abukawa *et al* 1995, Kelly *et al* 1986). ARPES (Abukawa *et al* 1995), IPES (Hill and McLean 1997a, 1999) and STS (Kraft *et al* 1997) measurements of single-domain surfaces have shown three 1D metallic surface states (m_1–m_3), dispersing upward from the BZ boundary, and crossing E_F. The half-filled m_3 band originates from Si–In bonds. It has a strong 1D character, and forms a nearly ideal flat FS. m_2 and m_3 are bonding and antibonding combinations of p_z orbitals on two adjacent In chains, with filling factors of 0.1 and 0.4. They exhibit a much lower anisotropy and strongly warped FSs. T-dependent measurements, including possibly the first real space observation of a CDW in an atomic wire, revealed that this structure is not stable (Yeom *et al* 1999). At low temperature the periodicity is doubled. ARPES shows the absence of a Fermi level crossing, and the reduction of the spectral intensities of all three bands near E_F. This was nonetheless interpreted as the result of a 1D CDW transition driven only by the half-filled m_3 state, with an estimated Peierls gap of 100–200 meV. Due to the finite 2D interchain coupling, the true low-temperature ground state should have an (8 × 2) periodicity, with the CDWs on different chains locked in phase. Other ARPES results suggest that both m_2 and m_3 states may be involved in the transition, and that below T_c charge is transferred from m_1 to the other two bands, which rigidly shift to higher energies (Gallus *et al* 2001). Since a single nesting vector cannot be responsible for the simultaneous opening of a gap in two bands, a more complex mechanism than a simple Peierls transition may be at work (Noguera 1986).

The rigid energy shift is not confirmed by other ARPES data, which show the opening of different gaps for the m_2 (150 ± 40 meV) and the m_3 (80 ± 10 meV) bands at low temperature (Yeom *et al* 2002). A novel gap opening mechanism for this triple-band Peierls system has been proposed based on recent temperature-dependent ARPES results (Ahn *et al* 2004a). A complete mapping of the BZ (figure 14) shows that, at low temperature, charge is transferred between the closely related m_1 and m_2 bands, until the former is totally depopulated and $k_F(m_2) \approx k_F(m_3)$. The Peierls transition is mainly driven by the well nested 1D FS of m_3 but, due to the very close Fermi wavevectors, m_2 is also involved in the transition. This is confirmed by the observation that the gap size of m_2 is largest at the boundary of the ×2 BZ. These results underline the importance of interband interactions in multiband Peierls systems. The Si(111)(4 × 1)–In interface behaves as a 1D CDW system with two 'competing' metallic bands. On the other hand, the finite intensity measured at E_F above T_c excludes an interpretation in terms of an LL. ARPES and core-level measurements have also been performed to test a quite different theoretical scenario, which associates the high-T metallic phase with intermediate metallic configurations between two degenerate and fluctuating insulating (8 × 2) ground states (González *et al* 2006). The data do not show the spectral broadening expected from this model with increasing temperature. Therefore, they exclude structural or electronic fluctuations within the timescale ($\approx fs$) of the photoemission process. Nevertheless, the MI transition could still be a cooperative phenomenon where the structural transition within the In chains modifies the band structure, thus setting the stage for the electronic instability, and for the abrupt opening of the Peierls gap (Sun *et al* 2008).

4.4. Metal overlayers on Si(100)

Si(100)–group-III metals

The Si(100) surface exhibits a well known (2 × 1) surface reconstruction which consists of both symmetric and buckled Si dimers (Hamers *et al* 1986). The adsorption of group-III metals leads to the formation of well ordered chain-like structures at submonolayer coverages (Yeom *et al* 1995b, Evans and Nogami 1999, Dong *et al* 1997). These quasi-1D nanostructures have been investigated for exotic and non-Fermi-liquid signatures.

Metal deposition at $T < 350\,^{\circ}$C and increasing coverages up to 0.5 ML yields surface structures with (2 × 3), (2 × 5) and finally (2 × 2) periodicities (Yeom *et al* 1995a, Sakama *et al* 1996b, 1993). The well ordered (2 × 2) phase at 0.5 ML corresponds to a complete saturation of the dangling bonds of the dimerized Si(100) substrate. After a long debate about the detailed atomic structure of the 1D chains, it is now generally believed that the group-III adsorbates form symmetric metal ad-dimers, which are located in the troughs between the underlying Si dimer rows and are oriented parallel to the Si dimers (Dong *et al* 1997, Itoh *et al* 1994a, Northrup *et al* 1991, Brocks *et al* 1993, Steele *et al* 1993, Itoh *et al* 1993, Qian *et al* 1994, Tang *et al* 1995, Gupta and Batra 2004, Park *et al* 2005). ARPES data have shown that the

Si(100)(2×2)–(group-III metal) interfaces are semiconducting, with a bandgap > 0.6 eV (Northrup *et al* 1991, Yeom *et al* 1996a), in agreement with STM/STS results (Sakama *et al* 1996a). The bandgap corresponds to the bonding–antibonding splitting of the covalent ad-dimer bonds (Yeom 2001, 1998). Four additional surface states, assigned to metal–Si backbonds, are observed in the Si bulk bandgap (Yeom *et al* 1996a, 1996b, 1994). The dispersions of the surface states, and their anisotropies between the directions parallel and perpendicular to the ad-dimer chains, are both small.

The electronic structure of the (2 × 3) phase is almost identical except for an additional fully occupied surface state which is assigned to the remaining dangling bonds of the Si dimers (Enta *et al* 1991, Yeom *et al* 1997). It was suggested that a Peierls mechanism might contribute to the formation of the dimerized structure and to the surface bandgap (Dong *et al* 1997), but a serious difficulty with this interpretation is the absence of a clear energy gap around E_F for $k = \pi/2$ (Yeom 1998). Although it is believed that free-standing nanowires would be metallic, and subject to an MI Peierls transition, the interaction with the Si(100) substrate clearly affects the 1D electronic structure, reducing and masking the effects of the Peierls instability (Dong *et al* 1998).

Thallium is anomalous among group-III elements. Due to the so-called 'inert-pair effect' of the 6s orbital, it exhibits both trivalency and monovalency (Greenwood and Earnshaw 1984). This is namely true for adsorption on Si(100)(2 × 1), where Tl behaves as a typical group-III metal for a 0.5 ML coverage, but as a monovalent alkali metal for 0.25, 0.75 and 1.0 ML (Saranin *et al* 2005a). The induced 1D (2 × 2) reconstruction at $\Theta = 0.5$ ML is identical to that of other group-III elements (Visikovsky *et al* 2005). The 1D (2 × 1) reconstruction at a coverage of 1.0 ML has been found to undergo a temperature-induced order–disorder transition. ARPES measurements at RT have revealed the absence of surface states crossing the Fermi level (Saranin *et al* 2005b). Therefore, the low-temperature reconstruction cannot be the result of an FS driven instability.

Si(100)–group-IV metals

Similar to the case of group-III elements, RT adsorption of group-IV metals (Sn and Pb) on clean Si(100)(2 × 1) induces the formation of isolated dimer chains oriented parallel to the underlying Si dimers at submonolayer coverages (Itoh *et al* 1994b, Veuillen *et al* 1996, Yoon *et al* 2003, Baski *et al* 1991, Glueckstein *et al* 1998). Again, the spacing between these rows decreases with increasing coverage, until regions with a (2 × 2) symmetry form near 0.5 ML (Baski *et al* 1991, Zhao *et al* 1992, Li *et al* 1994). It has been shown by STM and LEED that this interface is more disordered than the (2 × 2) reconstruction induced by group-III metals (Glueckstein *et al* 1998). Simple electron counting predicts that group-IV ad-dimers should be buckled and asymmetric since there remains one dangling bond per atom after each adatom is connected to the substrate and to the other atom of the dimer. The above prediction is supported by theoretical (González-Méndez and Takeuchi 1998, Zhu *et al* 2006) and experimental studies (Itoh *et al* 1994b, Glueckstein *et al* 1998, Dong *et al* 2001, 2000). The electronic properties of the Sn and Pb dimer chains have been studied by ARPES (Le Lay *et al* 1989, Tono *et al* 2000), IPES (Pedio *et al* 1994), and STS (Magaud *et al* 2002). The 1D chains are semiconducting ($\Delta > 0.5$ eV) due to the local covalent bonding, surface dimerization and the buckling of the metal ad-dimers. The possible role of a Peierls instability has been also evoked (Dong *et al* 2001).

Unlike the homogeneous group-III and group-IV metal ad-dimers, mixed dimers should be metallic since they carry an odd number of electrons per atom (Magaud *et al* 2002). While ARPES results have not been reported yet, the stability of mixed In–Sn dimers on a Si(100)(2 × 1) substrate has been investigated by STM (Juré *et al* 2000) and first-principles calculations (Magaud *et al* 2002). The lowest-energy structure involves a doubling of the unit cell and charge transfer between dimers, and is expected to be insulating, in agreement with the predicted instability of 1D metals. On the other hand, the STM data indicate that, although In and Sn dimers co-exist in the same chain, mixed In–Sn dimers are found only as a minority species.

5. Conclusions

The interest in the electronic structure of quasi-1D systems has been steadily growing since the first experimental observations of their unusual and exciting properties. State-of-the-art spectroscopic measurements, namely by high energy and momentum resolution ARPES, provide a detailed view of the relevant electronic states. Much experimental work has been performed in the past decade covered by the present review. It was equally devoted to the study of bulk compounds, and of artificial 1D structures at surfaces. The former, besides showing some of the peculiar 1D electronic properties predicted by theory, are often also very interesting materials *per se*, with exciting broken-symmetry ground states. It is expected that increasingly accurate ARPES experiment on known and new compounds will be performed in the future. Complementary measurements employing novel probes of the electronic structure, notably synchrotron radiation based techniques like the rapidly developing high resolution resonant inelastic x-ray scattering (RIXS), will also contribute to a better understanding of their properties.

Atomic wires at metal and semiconductor surfaces are a subject of strong ongoing interest in surface science. Recent results have demonstrated the considerable advantages of bringing together a k-resolved probe like ARPES and a local probe like STM/STS. Although technically challenging, this development can be expected to continue with the further integration of the two techniques in more complex experiments. These artificial structures also represent model systems where accurate tests of theoretical predictions should be possible, while tuning crucial physical parameters like the strength of electronic correlations and of transverse interactions. One can anticipate a growing activity in this direction. The future discovery of new 1D nanostructures, and the use of a wider range of substrates with different band structures, bonding characters, and electron densities, is

likely to open new exciting opportunities for research in one-dimensional physics.

Acknowledgments

It is a pleasure to acknowledge past co-workers at Lausanne, especially F Zwick and L Perfetti. EF acknowledges the Alexander S Onassis Public Benefit Foundation for the award of a scholarship. This work is supported by the Swiss National Science Foundation and by the MaNEP NCCR.

References

Abukawa T, Sasaki M, Hisamatsu F, Goto T, Kinoshita T, Kakizaki A and Kono S 1995 *Surf. Sci.* **325** 33
Ahn J R, Byun J H, Koh H, Rotenberg E, Kevan S D and Yeom H W 2004a *Phys. Rev. Lett.* **93** 106401
Ahn J R, Choi W H, Kim Y K, Lee H S and Yeom H W 2003a *Phys. Rev.* B **68** 165314
Ahn J R, Kang P G, Ryang K D and Yeom H W 2005 *Phys. Rev. Lett.* **95** 196402
Ahn J R, Kim N D, Lee S S, Lee K D, Yu B D, Jeon D, Kong K and Chung J W 2002a *Europhys. Lett.* **57** 859
Ahn J R, Kim Y J, Lee H S, Hwang C C, Kim B S and Yeom H W 2002b *Phys. Rev.* B **66** 153403
Ahn J R, Yeom H W, Cho E S and Park C Y 2004b *Phys. Rev.* B **69** 233311
Ahn J R, Yeom H W, Yoon H S and Lyo I W 2003b *Phys. Rev. Lett.* **91** 196403
Allen J W 2002 *Solid State Commun.* **123** 469–87
Altmann K N, Crain J N, Kirakosian A, Lin J L, Petrovykh D Y, Himpsel F J and Losio R 2001 *Phys. Rev.* B **64** 035406
An T, Yoshimura M, Ono I and Ueda K 2000 *Phys. Rev.* B **61** 3006–11
Ando H, Yokoya T, Ishizaka K, Tsuda S, Kiss T, Shin S, Eguchi T, Nohara M and Takagi H 2005 *J. Phys.: Condens. Matter* **17** 4935–40
Barke I, Zheng F, Rügheimer T and Himpsel F 2006 *Phys. Rev. Lett.* **97** 226405
Barth J, Costantini G and Kern K 2005 *Nature* **437** 671
Barth J V, Brune H, Ertl G and Behm R J 1990 *Phys. Rev.* B **42** 9307–18
Baski A, Erwin S and Whitman L 1995 *Science* **269** 1556–60
Baski A A, Quate F Q and Nogami J 1991 *Phys. Rev.* B **44** 11167–77
Baumberger F, Greber T, Delley B and Osterwalder J 2002 *Phys. Rev. Lett.* **88** 237601
Baumberger F, Hengsberger M, Muntwiler M, Shi M, Krempasky J, Patthey L, Osterwalder J and Greber T 2004a *Phys. Rev. Lett.* **92** 196805
Baumberger F, Hengsberger M, Muntwiler M, Shi M, Krempasky J, Patthey L, Osterwalder J and Greber T 2004b *Phys. Rev. Lett.* **92** 016803
Berge K, Gerlach A, Meister G, Goldmann A and Bertel E 2004 *Phys. Rev.* B **70** 155303
Bertel E and Lehmann J 1998 *Phys. Rev. Lett.* **80** 1497–500
Brocks G, Kelly P and Car R 1993 *Phys. Rev. Lett.* **70** 2786–9
Bromberger C, Crain J N, Altmann K N, Paggel J J, Himpsel F J and Fick D 2003 *Phys. Rev.* B **68** 075320
Brune H, Giovannini M, Bromann K and Kern K 1998 *Nature* **394** 451
Bulut N, Matsueda H, Tohyama T and Maekawa S 2006 *Phys. Rev.* B **74** 113106
Burgi L, Brune H, Jeandupeux O and Kern K 1999 *Phys. Rev. Lett.* **82** 4516
Burgi L, Brune H, Jeandupeux O and Kern K 2000 *J. Electron Spectrosc. Relat. Phenom.* **109** 33–49
Bychkov Y and Rashba E 1984 *JETP Lett.* **39** 78–81
Carpinelli J M and Weitering H H 1996 *Phys. Rev.* B **53** 12651–4
Cercellier H, Fagot-Revurat Y, Kierren B, Reinert F, Popović D and Malterre D 2004 *Phys. Rev.* B **70** 193412
Choi W H, Kang P G, Ryang K D and Yeom H W 2008 *Phys. Rev. Lett.* **100** 126801
Claessen R, Sing M, Schwingenschlögl U, Blaha P, Dressel M and Jacobsen C S 2002 *Phys. Rev. Lett.* **88** 096402
Collins I R, Moran J T, Andrews P, Cosso R, O'Mahony J D, McGilp J F and Margaritondo G 1995 *Surf. Sci.* **345** 45
Crain J N, Kirakosian A, Altmann K N, Bromberger C, Erwin S C, McChesney J L, Lin J L and Himpsel F J 2003 *Phys. Rev. Lett.* **90** 176805
Crain J N, McChesney J L, Zheng F, Gallagher M C, Snijders P C, Bissen M, Gundelach C, Erwin S C and Himpsel F J 2004 *Phys. Rev.* B **69** 125401
Crampin S, Kröger J, Jensen H and Berndt R 2005 *Phys. Rev. Lett.* **95** 029701
Crommie M, Lutz C and Eigler D 1993a *Science* **262** 218–20
Crommie M F, Lutz C P and Eigler D M 1993b *Nature* **363** 524–7
Daimon H and Ino S 1985 *Surf. Sci.* **164** 320–6
Dardel B, Malterre D, Grioni M, Weibel P, Baer Y and Lévy F 1991 *Phys. Rev. Lett.* **67** 3144–7
Deisl C, Swamy K, Memmel N, Bertel E, Franchini C, Schneider G J R, Walter S, Hammer L and Heinz K 2004 *Phys. Rev.* B **69** 195405
Denlinger J D, Gweon G H, Allen J W, Olson C G, Marcus J, Schlenker C and Hsu L S 1999 *Phys. Rev. Lett.* **82** 2540–3
Desjonquères M C, Spanjaard D, Barreteau C and Raouafi F 2002 *Phys. Rev. Lett.* **88** 056104
Dessau D S, Saitoh T, Park C H, Shen Z X, Villella P, Hamada N, Moritomo Y and Tokura Y 1998 *Phys. Rev. Lett.* **81** 192–5
Didiot C, Fagot-Revurat Y, Pons S, Kierren B, Chatelain C and Malterre D 2006 *Phys. Rev.* B **74** R81404
Didiot C, Pons S, Kierren B, Fagot-Revurat Y and Malterre D 2007 *Nat. Nanotechnol.* **2** 617–21
Dong Z C, Fujita D and Nejoh H 2001 *Phys. Rev.* B **63** 115402
Dong Z C, Yakabe T, Fujita D, Jiang Q D and Nejo H 1997 *Surf. Sci.* **380** 23–30
Dong Z C, Yakabe T, Fujita D, Jiang Q D and Nejo H 1998 *Surf. Sci.* **415** 301–2
Dong Z C, Fujita D, Yakabe T, Sheng H and Nejoh H 2000 *J. Vac. Sci. Technol.* B **18** 2371–6
Dressel M 2003 *Naturwissenschaften* **90** 337–44
Dzyaloshinskii I 2003 *Phys. Rev.* B **68** 085113
Eguchi R, Yokoya T, Kiss T, Ueda Y and Shin S 2002 *Phys. Rev.* B **65** 205124
Enta Y, Suzuki S and Kono S 1991 *Surf. Sci.* **242** 277–83
Erwin S C 1995 *Phys. Rev. Lett.* **75** 1973–6
Erwin S C and Weitering H H 1998 *Phys. Rev. Lett.* **81** 2296–9
Evans M M R and Nogami J 1999 *Phys. Rev.* B **59** 7644–8
Fedorov A V, Brazovskii S A, Muthukumar V N, Johnson P D, Xue J, Duda L C, Smith K E, McCarroll W H, Greenblatt M and Hulbert S L 2000 *J. Phys.: Condens. Matter* **12** L191–8
Fölsch S, Hyldgaard P, Koch R and Ploog K H 2004 *Phys. Rev. Lett.* **92** 056803
Fujimori S I, Ino A, Okane T, Fujimori A, Okada K, Manabe T, Yamashita M, Kishida H and Okamoto H 2002 *Phys. Rev. Lett.* **88** 247601
Fujisawa H, Yokoya T, Takahashi T, Miyasaka S, Kibune M and Takagi H 1998 *Solid State Commun.* **106** 543–7
Gallus O, Pillo T, Hengsberger M, Segovia P and Baer Y 2001 *Eur. Phys. J.* B **20** 313–9
Gambardella P, Dallmeyer A, Maiti K, Malagoli M C, Eberhardt W, Kern K C and Carbone C 2002 *Nature* **416** 301–4
Giamarchi T 2003 *Quantum Physics in One Dimension* (Oxford: Clarendon)
Glueckstein J C, Evans M M R and Nogami J 1998 *Surf. Sci.* **415** 80–94
González C, Flores F and Ortega J 2006 *Phys. Rev. Lett.* **96** 136101

Gonzalez-Lakunza N, Fernández-Torrente I, Franke K J, Lorente N, Arnau A and Pascual J I 2008 *Phys. Rev. Lett.* **100** 156805

González-Méndez M E and Takeuchi N 1998 *Phys. Rev.* B **58** 16172–6

Gotoh Y and Ino S 1978 *Japan. J. Appl. Phys.* **17** 2097–109

Greenwood N N and Earnshaw A 1984 *Chemistry of the Elements* (London: Pergamon)

Grioni M, Berger H, Garnier M, Bommeli F, Degiorgi L and Schlenker C 1996 *Phys. Scr.* T **66** 172–6

Grüner G 1994 *Density Waves in Solids* (Reading, MA: Addison-Wesley)

Gupta B C and Batra I P 2004 *Phys. Rev.* B **69** 165322

Gurnett M, Gustafsson J B, Magnusson K O, Widstrand S M and Johansson L S O 2002 *Phys. Rev.* B **66** 161101

Gweon G H, Denlinger J D, Allen J W, Claessen R, Olson C G, Höchst H, Marcus J, Schlenker C and Schneemeyer L F 2001 *J. Electron Spectrosc. Relat. Phenom.* **117/118** 481–502

Gweon G H *et al* 1996 *J. Phys.: Condens. Matter* **8** 9923–38

Hager J, Matzdorf R, He J, Jin R, Mandrus D, Cazalilla M A and Plummer E W 2005 *Phys. Rev. Lett.* **95** 186402

Hamers R J, Tromp R M and Demuth J E 1986 *Phys. Rev.* B **34** 5343–57

Hansmann M, Pascual J I, Ceballos G, Rust H P and Horn K 2003 *Phys. Rev.* B **67** 121409

Hengsberger M, Purdie P, Segovia P, Garnier M and Baer Y 1999 *Phys. Rev. Lett.* **83** 592–5

Higashiguchi M, Shimada K, Arita M, Miura Y, Tobita N, Cui X Y A, Namatame H and Taniguchi M 2007 *Surf. Sci.* **601** 4005–9

Hill I G and McLean A B 1997a *Phys. Rev.* B **56** 15725–8

Hill I G and McLean A B 1997b *Phys. Rev.* B **55** 15664–8

Hill I G and McLean A B 1999 *Phys. Rev.* B **59** 9791–3

Himpsel F, Altmann K, Crain J, Kirakosian A, Lin J and Liebsch A 2002 *J. Electron Spectrosc. Relat. Phenom.* **126** 89–99

Hoinkis M *et al* 2005 *Phys. Rev.* B **72** 125127

Hörmandinger G and Pendry J B 1994 *Phys. Rev.* B **50** 18607–20

Hüfner S, Claessen R, Reinert F, Straub T, Strocov V N and Steiner P 1999 *J. Electron Spectrosc. Relat. Phenom.* **100** 191–213

Ichikawa T and Ino S 1980 *Surf. Sci.* **97** 489–502

Ignatiev P, Stepanyuk V, Klavsyuk A, Hergert W and Bruno P 2007 *Phys. Rev.* B **75** 155428

Ino S 1987 *Reflection High-Energy Electron Diffraction and Reflection Electron Imaging of Surfaces* (*NATO AS1 Series B: Phys.* vol 18) (New York: Plenum)

Ito T, Chainani A, Haruna T, Kanai K, Yokoya T, Shin S and Kato R 2005 *Phys. Rev. Lett.* **95** 246402

Itoh H, Itoh J, Schmid A and Ichinokawa T 1993 *Phys. Rev.* B **48** 14663–6

Itoh H, Itoh J, Schmid A and Ichinokawa T 1994a *Surf. Sci.* **302** 295–302

Itoh H, Tanabe H, Winau D, Schmid A K and Ichinokawa T 1994b *J. Vac. Sci. Technol.* B **12** 2086–9

Jalochowski M, StroZak M and Zdyb R 1997 *Surf.Sci.* **375** 203

Jeong S and Kang M H 1995 *Phys. Rev.* B **51** 17635–41

Jeong S and Kang M H 1996 *Phys. Rev.* B **54** 8196–201

Juré L, Magaud L, Mallet P and Veuillen J Y 2000 *Appl. Surf. Sci* **162/163** 638–43

Kang M H, Kang J H and Jeong S 1998 *Phys. Rev.* B **58** R13359–62

Kelly M, Margaritondo G, Anederson J, Frankel D and Lapeyre G 1986 *J. Vac. Sci. Technol.* A **4** 1396–9

Kern K, Niehus H, Schatz A, Zeppenfeld P, Goerge J and Comsa G 1991 *Phys. Rev. Lett.* **67** 855–8

Kidd T E, Valla T, Johnson P D, Kim K W, Gu G D and Homes C C 2008 *Phys. Rev.* B **77** 054503

Kim B J *et al* 2006 *Nat. Phys.* **2** 397–401

Kim C, Matsuura A Y, Shen Z X, Motoyama N, Eisaki H, Uchida S, Tohyama T and Maekawa S 1996 *Phys. Rev. Lett.* **77** 4054–7

Kim C, Shen Z X, Motoyama N, Eisaki H, Uchida S, Tohyama T and Maekawa S 1997 *Phys. Rev.* B **56** 15589–95

Kliewer J, Berndt R, Chulkov E, Silkin V, Echenique P and Crampin S 2000 *Science* **288** 1399–402

Kobayashi K, Mizokawa T, Fujimori A, Isobe M and Ueda Y 1998 *Phys. Rev. Lett.* **80** 3121–4

Kraft J, Ramsey M G and Netzer F P 1997 *Phys. Rev.* B **55** 5384–93

Kröger J 2006 *Rep. Prog. Phys.* **69** 899–969

Kulawik M, Nilius N and Freund H 2006 *Phys. Rev. Lett.* **96** 036103

Kuntscher C A, Gerhold S, Nücker N, Cummins T R, Lu D H, Schuppler S, Gopinath C S, Lichtenberg F, Mannhart J and Bohnen K P 2000 *Phys. Rev.* B **61** 1876–83

Kuntscher C A, Schuppler S, Haas P, Gorshunov B, Dressel M, Grioni M, Lichtenberg F, Herrnberger A, Mayr F and Mannhart J 2002 *Phys. Rev. Lett.* **89** 236403

LaShell S, McDougall B and Jensen E 1996 *Phys. Rev. Lett.* **77** 3419–22

Lau K H and Kohn W 1978 *Surf. Sci.* **75** 69–85

Lee K D and Chung J 1998 *Phys. Rev.* B **57** R2053–6

Le Lay G, Hricovini K and Bonnet J E 1989 *Phys. Rev.* B **39** 3927–30

Lee P A, Rice T M and Anderson P W 1973 *Phys. Rev. Lett.* **31** 462–5

Lee S S, Kim N D, Hwang C G, Song H J and Chung J W 2002 *Phys. Rev.* B **66** 115317

Li J, Schneider W D, Berndt R, Bryant O R and Crampin S 1998 *Phys. Rev. Lett.* **81** 4464–7

Li J L, Jia J F, Liang X J, Liu X, Wang J Z, Xue Q K, Li Z Q, Tse J S, Zhang Z and Zhang S B 2002 *Phys. Rev. Lett.* **88** 066101

Li L, Koziol C, Wurm K, Hong Y, Bauer E and Tsong I S T 1994 *Phys. Rev.* B **50** 10834–42

Losio R, Altmann K N and Himpsel F J 2000 *Phys. Rev. Lett.* **85** 808–11

Losio R, Altmann K N, Kirakosian A, Lin J L, Petrovykh D Y and Himpsel F J 2001 *Phys. Rev. Lett.* **86** 4632–5

Magaud L, Pasturel A and Veuillen J Y 2002 *Phys. Rev.* B **65** 245306

Mahan J D 1986 *Many-Particle Physics* (New York: Plenum)

Malterre D, Kierren B, Fagot-Revurat Y, Pons S, Tejeda A, Didiot C, Cercellier H and Bendounan A 2007 *New J. Phys.* **9** 391

Matsuda I, Hengsberger M, Baumberger F, Greber T, Yeom H W and Osterwalder J 2003 *Phys. Rev.* B **68** 195319

McChesney J, Crain J, Himpsel F and Bennewitz R 2005 *Phys. Rev.* B **72** 35446

McChesney J L, Crain J N, Pérez-Dieste V, Zheng F, Gallagher M C, Bissen M, Gundelach C and Himpsel F J 2004 *Phys. Rev.* B **70** 195430

Meden V and Schonhammer K 1992 *Phys. Rev.* B **46** 15753–60

Menzel A, Zhang Z, Minca M, Bertel E, Redinger J and Zucca R 2006 *J. Phys. Chem. Sol.* **67** 254–8

Menzel A, Zhang Z, Minca M, Loerting T, Deisl C and Bertel E 2005 *New J. Phys.* **7** 102

Mimura K, Wakita K, Arita M, Mamedov F, Orudzhev G, Taguchi Y, Ichikawa K, Namatame H and Taniguchi M 2007 *J. Electron Spectrosc. Relat. Phenom.* **156–158** 379–82

Minca M, Penner S, Dona E, Menzel A, Bertel E, Brouet V and Redinger J 2007 *New J. Phys.* **9** 386

Mishchenko A S and Nagaosa N 2004 *Phys. Rev. Lett.* **93** 036402

Mitrovic S, Perfetti L, Søndergaard C, Margaritondo G, Grioni M, Barišić N, Forró L and Degiorgi L 2004 *Phys. Rev.* B **69** 035102

Moritz H, Stoferle T, Gunter K, Kohl M and Esslinger T 2005 *Phys. Rev. Lett.* **94** 210401

Mozos J L, Ordejón P and Canadell E 2002 *Phys. Rev.* B **65** 233105

Mugarza A, Mascaraque A, Repain V, Rousset S, Altmann K N, Himpsel F, Koroteev Y M, Chulkov E V, de Abajo F G and Ortega J 2002 *Phys. Rev.* B **66** 245419

Mugarza A and Ortega J E 2003 *J. Phys.: Condens. Matter* **15** S3281–310

Mugarza A, Ortega J, Himpsel F and de Abajo F G 2003 *Phys. Rev.* B **67** 081404
Nagira M *et al* 2007a *Sur. Sci.* **61** 4041–4
Nagira M *et al* 2007b *Surf. Sci.* **401** 5254–7
Néel N, Kröger J and Berndt R 2006 *Adv. Mater.* **18** 174–7
Nilius N, Wallis T M and Ho W 2002 *Science* **297** 1853
Noguera C 1986 *J. Phys. C: Solid State Phys.* **19** 2161
Northrup J E, Schabel M C, Karlsson C J and Uhrberg R I G 1991 *Phys. Rev.* B **44** 13799–802
Nozières P 1964 *Interacting Fermi Systems* (New York: Benjamin)
Okazaki K, Fujimori A, Yamauchi T and Ueda Y 2004 *Phys. Rev.* B **69** 140506
Okazaki K, Tanaka K, Matsumo J, Fujimori A, Mattheiss L F, Iida S, Kerimova E and Namedov N 2001 *Phys. Rev.* B **64** 045210
Okuda T, Daimon H, Suga S, Tezuka Y and Ino S 1997a *Appl. Surf. Sci.* **121** 89–97
Okuda T, Daimon H, Suga S Y T and Ino S 1997b *Appl. Surf. Sci* **121** 87–9
Okuda T, Sakamoto K, Nishimoto H, Daimon H, Suga S, Kinoshita T and Kakizaki A 1997c *Phys. Rev.* B **55** 6762–5
Okuda T, Shigeoka H, Daimon H, Suga S, Kinoshita T and Kakizaki A 1994 *Surf. Sci.* **321** 105–10
Ortega J E, Mugarza A, Pérez-Dieste V, Repain V, Rousset S and Mascaraque A 2002 *Phys. Rev.* B **65** 165413
Ortega J E, Ruiz-Osés M, Cordón J, Mugarza A, Kuntze J and Schiller F 2005 *New J. Phys.* **7** 101
Ortega J E, Speller S, Bachmann A R, Mascaraque A, Michel E G, Närmann A, Mugarza A, Rubio A and Himpsel F J 2000 *Phys. Rev. Lett.* **84** 6110–3
Pampuch C, Rader O, Kachel T, Gudat W, Carbone C, Kläsges R, Bihlmayer G, Blügel S and Eberhardt W 2000 *Phys. Rev. Lett.* **85** 2561–4
Papagno M, Pacilé D, Caimi G, Berger H, Degiorgi L and Grioni M 2006 *Phys. Rev.* B **73** 115120
Park J Y, Seo J H, Whang C N, Kim S S, Choi D S and Chae K H 2005 *J. Chem. Phys.* **122** 244723
Pedio M, Ghisalberti V, Ottaviani C, Capozi M, Lama F, Quaresima C and Perfetti P 1994 *Surf. Sci.* **303** 153–60
Pennec Y, Auwärter W, Schiffrin A, Weber-Bargioni A, Riemann A and Barth J V 2007 *Nat. Nanotechnol.* **2** 99–103
Perebeinos V and Allen P B 2000 *Phys. Rev. Lett.* **85** 5178–81
Perfetti L, Berger H, Reginelli A, Degiorgi L, Höchst H, Voit J, Margaritondo G and Grioni M 2001 *Phys. Rev. Lett.* **87** 216404
Perfetti L, Mitrovic S, Margaritondo G, Grioni M, Forró L, Degiorgi L and Höchst H 2002 *Phys. Rev.* B **66** 075107
Perucchi A, Sondergaard C, Mitrovic S, Grioni M, Barisic N, Berger H, Forró L and Degiorgi L 2004 *Eur. Phys. J.* B **39** 433–40
Pons S, Mallet P, Magaud L and Veuillen J Y 2003 *Europhys. Lett.* **61** 375–81
Qian Y, Bedzyk M J, Tang S, Freeman A J and Franklin G E 1994 *Phys. Rev. Lett.* **73** 1521–4
Reinert F, Nicolay G, Schmidt S, Ehm D and Hufner S 2001 *Phys. Rev.* B **63** 115415
Röttger B, Hanbücken M and Neddermeyer H 2001 *Appl. Surf. Sci* **162** 595–8
Sakama H, Kawazu A, Sueyoshi T, Sato T and Iwatsuki M 1996a *Phys. Rev.* B **54** 8756–60
Sakama H, Murakami K, Nishikata K and Kawazu A 1993 *Phys. Rev.* B **48** 5278–81
Sakama H, Murakami K, Nishikata K and Kawazu A 1996b *Phys. Rev.* B **53** 1080–2
Sakamoto K, Ashima H, Zhang H M and Uhrberg R I G 2001 *Phys. Rev.* B **65** 045305
Sakamoto K, Okuda T, Nishimoto H, Daimon H, Suga S, Kinoshita T and Kakizaki A 1994 *Phys. Rev.* B **50** 1725–32
Sánchez O, García J M, Segovia P, Alvarez J, Vázquez de Parga A L, Ortega J E, Prietsch M and Miranda R 1995 *Phys. Rev.* B **52** 7894–7
Sánchez-Portal D, Riikonen S and Martin R M 2004 *Phys. Rev. Lett.* **93** 146803
Saranin A A *et al* 2005a *Phys. Rev.* B **71** 035312
Saranin A A *et al* 2005b *Phys. Rev.* B **71** 165307
Schäfer J, Rotenberg E, Kevan S D, Blaha P, Claessen R and Thorne R E 2001 *Phys. Rev. Lett.* **87** 196403
Schäfer J, Sing M, Claessen R, Rotenberg E, Zhou X J, Thorne R E and Kevan S D 2003 *Phys. Rev. Lett.* **91** 066401
Schiller F, Ruiz-Osés M, Cordón J and Ortega J E 2005 *Phys. Rev. Lett.* **95** 066805
Segovia P, Purdie P, Hengsberger M and Baer Y 1999 *Nature* **402** 504
Shen K M *et al* 2004 *Phys. Rev. Lett.* **93** 267002
Shiraki S, Fujisawa H, Nantoh M and Kawai M 2004 *Phys. Rev. Lett.* **92** 96102
Shockley W 1939 *Phys. Rev.* **56** 317–23
Silly F, Pivetta M, Ternes M, Patthey F, Pelz J and Schneider W D 2004 *Phys. Rev. Lett.* **92** 16101
Sing M, Meyer J, Claessen R, Blaha P, Carmelo J M P, Martelo L M, Sacramento P D, Dressel M and Jacobsen C S 2003 *Phys. Rev.* B **68** 125111
Sing M, Schwingenschlögl U, Hoinkis M, Glawion S, Blaha P, Gavrila G, Jacobsen C S and Claessen R 2007 *Phys. Rev.* B **76** 245119
Smith N V, Thiry P and Petroff Y 1993 *Phys. Rev.* B **47** 15476
Snijders P, Rogge S and Weitering H 2006 *Phys. Rev. Lett.* **96** 76801
Søndergaard C, Mitrovic S and Grioni M 2003 *PSI-Scientific Report 2002* p 43
Sperl A, Kröger J, Néel N, Jensen H, Berndt R, Franke A and Pehlke E 2008 *Phys. Rev.* B **77** 085422
Starowicz P, Battaglia C, Clerc F, Despont L, Prodan A, van Midden H J P, Szerer U, Szytula A, Garnier M G and Aebi P 2007 *J. Alloys Compounds* **442** 268–71
Steele B E, Li L, Stevens J L and Tsong I S T 1993 *Phys. Rev.* B **47** 9925–7
Suga S *et al* 2004 *Phys. Rev.* B **70** 155106
Sun Y J, Agario A, Souma S, Sugawara K, Tago Y, Sato T and Takahashi T 2008 *Phys. Rev.* B **77** 125115
Tamai A, Seitsonen A, Greber T and Osterwalder J 2006 *Phys. Rev.* B **74** 085407
Tang S, Freeman A J, Qian Y, Franklin G E and Bedzyk M J 1995 *Phys. Rev.* B **51** 1593–600
Tono K, Yeom H W, Matsuda I and Ohta T 2000 *Phys. Rev.* B **61** 15866–72
Varykhalov A and Gudat W 2005 *Phys. Rev.* B **72** 241404
Varykhalov A, Rader O and Gudat W 2005 *Phys. Rev.* B **72** 115440
Vescoli V, Zwick F, Voit J, Berger H, Zacchigna M, Degiorgi L, Grioni M and Grüner G 2000 *Phys. Rev. Lett.* **84** 1272–5
Veuillen J Y, Gomez-Rodriguez J M and Cinti R C 1996 *J. Vac. Sci. Technol.* B **14** 1010–4
Visikovsky A, Mizuno S and Tochihara H 2005 *Phys. Rev.* B **71** 245407
Vitali L, Wahl P, Schneider M, Kern K, Silkin V, Chulkov E and Echenique P 2003 *Surf. Sci.* **523** L47–52
Voit J 1993 *J. Phys.: Condens. Matter* **5** 8305–36
Voit J 1994 *Rep. Prog. Phys.* **57** 977–1116
Voit J 1998 *Eur. Phys. J.* B **5** 505–19
Voit J, Perfetti L, Zwick F, Berger H, Margaritondo G, Grüner G, Höchst H and Grioni M 2000 *Science* **290** 501–3
Wan K J, Lin X F and Nogami J 1992 *Phys. Rev.* B **46** 13635–8
Wang F, Alvarez J V, Mo S-K, Allen J W, Gweon G-H, He J, Jin R, Mandrus D and Höchst H 2006 *Phys. Rev. Lett.* **96** 196403
Weitering H H, DiNardo N J, Pérez-Sandoz R, Chen J and Mele E J 1994 *Phys. Rev.* B **49** 16837–40
Weitering H H, Shi X and Erwin S C 1996 *Phys. Rev.* B **54** 10585–92
Whangbo M H, Canadell E, Foury P and Pouget J P 1991 *Science* **252** 96–8
Wilson R J and Chiang S 1987 *Phys. Rev. Lett.* **58** 369–72

Xue J, Duda L C, Smith K E, Fedorov A V, Johnson P D, Hulbert S L, McCarroll W and Greenblatt M 1999 *Phys. Rev. Lett.* **83** 1235–8
Yeom H W 1998 *Surf. Sci.* **415** 299–300
Yeom H W 2001 *J. Electron. Spectrsc. Relat. Phenom.* **114–116** 283–90
Yeom H W, Abukawa T, Nakamura M, Chen X, Suzuki S, Sato S, Sakamoto K, Sakamoto T and Kono S 1995a *Surf. Sci.* **340** L983–7
Yeom H W, Abukawa T, Nakamura M, Suzuki S, Sato S, Sakamoto K, Sakamoto T and Kono S 1995b *Surf. Sci.* **341** 328–34
Yeom H W, Abukawa T, Takakuwa Y, Mori Y, Shimatani T, Kakizaki A and Kono S 1996a *Phys. Rev.* B **53** 1948–57
Yeom H W, Abukawa T, Takakuwa Y, Mori Y, Shimatani T, Kakizaki A and Kono S 1997 *Phys. Rev.* B **55** 15669–74
Yeom H W, Abukawa T, Takakuwa Y, Nakamura M, Kimura A, Shimatani T, Mori Y, Kakizaki A and Kono S 1996b *J. Electron. Spectrsc. Relat. Phenom.* **80** 177–80
Yeom H W, Abukawa T, Takakuwa Y, Nakamura M, Kimura M, Kazikazi A and Kono S 1994 *Surf. Sci.* **321** L177–82
Yeom H W, Ahn J R, Yoon H S, Lyo I W, Jeong H and Jeong S 2005 *Phys. Rev.* B **72** 035323
Yeom H W, Horikoshi K, Zhang H M, Ono K and Uhrberg R I G 2002 *Phys. Rev.* B **65** 241307
Yeom H W *et al* 1999 *Phys. Rev. Lett.* **82** 4898–901
Yokoya T, Kiss T, Chainani A, Shin S and Yamaya K 2005 *Phys. Rev.* B **71** 140504
Yoon H S, Park S J, Lee J E, Whang C N and Lyo I W 2004 *Phys. Rev. Lett.* **92** 096801
Yoon H S, Ryu M A, Han K H and Lyo I W 2003 *Surf. Sci.* **547** 210–8
Zhao R G, Jia J F and Yang W S 1992 *Surf. Sci.* **274** L519–23
Zhu Y, Ye L and Wang X 2006 *J. Appl. Phys.* **100** 083703
Zwick F, Brown S, Margaritondo G, Merlic C, Onellion M, Voit J and Grioni M 1997 *Phys. Rev. Lett.* **79** 3982–5
Zwick F, Jérome D, Margaritondo G, Onellion M, Voit J and Grioni M 1998 *Phys. Rev. Lett.* **81** 2974–7